In vivo isogenic modelling unveils *TP53*-associated relapse trajectories in T-cell acute lymphoblastic leukemia

Stéphanie Gachet[1,2,3,#], Samuel Quentin[1,2,4*], Lucie Hernandez[1,2*], Loïc Maillard[1,2], Marie Passet[1,2,4], Rathana Kim[1,2,3,4], Hugo Bergugnat[1,2], Melha Benlebna[1,2], Rémy Jelin[5], Marine Aglave[5], Maxime Boy[1,2], Véronique Parietti[1,2], Pierre Fenaux[6], André Baruchel[7], Hervé Dombret[1,4,6], Nicolas Boissel[1,2,3,8], François Sigaux[1,2,3,4], Hugues de Thé[1,2,3,4], Emmanuelle Clappier[1,2,3,4] and Jean Soulier[1,2,3,4].

[1]Institut de Recherche Saint-Louis (IRSL), Université Paris Cité, 75010 Paris, France;
[2]INSERM UMR1342 / CNRS EMR8000, Paris, France;
[3]Institut de la Leucémie, Hôpital Saint-Louis, APHP, Université Paris Cité, Paris, France;
[4]Hôpital Saint-Louis, Laboratoire d'Hématologie, APHP, Paris, France;
[5]Gustave Roussy, Département de la recherche, F-94805, Villejuif, France;
[6]Hôpital Saint-Louis, Département Hématologie Senior, APHP, Paris, France;
[7]Hôpital Robert Debré, APHP, Université Paris Cité, Paris, France;
[8]Hôpital Saint-Louis, Service d'Hématologie Adolescents et Jeunes Adultes, APHP, Paris, France.
[*]These co-authors contributed equally

Corresponding authors:
Drs. Stéphanie Gachet, PhD: stephanie.gachet@inserm.fr and Jean Soulier, MD, PhD: jean.soulier@aphp.fr

[#]Present address: Laboratoire des cellules Souches Hématopoïétiques et des Leucémies, Equipe Niche, Cancer et Radiations dans l'Hématopoïèse, Inserm U1274, Commissariat à l'Energie Atomique et aux Energies Alternatives (CEA), Université Paris-Saclay.

Running title:
TP53-altered relapse trajectories in T-ALL

Keywords: T-cell acute lymphoblastic leukemia, somatic *TP53* alterations, relapse, leukemia initiating cells, metabolic adaptation

Word counts:

Abstract, 150; Text, 3382

Number of Figures: 5

Footnotes:

Supplementary informations for this article (Supplementary Figures, 5 and Supplementary Tables, 3) are available online.

ABSTRACT

Many patients with T-cell acute lymphoblastic leukemia (T-ALL) relapse into a treatment-resistant disease. The mechanisms driving relapse remain largely elusive, in part due to the lack of faithful experimental models. Here, we leveraged patient-derived xenograft (PDX) pairs generated from diagnosis and relapse T-ALLs to functionally address the cellular mechanisms driving *TP53*-altered relapse. Beyond inter-T-ALL variability, comparative analyses revealed a unique, cell-intrinsic relapse phenotype that includes greater leukemia-initiating capacity and that can be conferred to diagnosis cells by *TP53* silencing. Transcriptomic profiling linked the relapse phenotype to deregulated OXPHOS metabolism and MYC signaling. Integration of single-cell profilings uncovered *TP53*-wildtype cell populations at diagnosis expressing a relapse profile, possibly reflecting a pre-existing modulation of *TP53* signaling. These cells sequentially evolved towards biallelic *TP53* inactivation at relapse. Collectively, our findings support a model in which T-ALL relapses emerge from a selected pre-existing transcriptional state characterized by deregulated metabolism that favors subsequent *TP53* inactivation.

INTRODUCTION

T-cell acute lymphoblastic leukemia (T-ALL) is an aggressive hematologic malignancy that represents 15% of pediatric and 25% of all adult ALL cases[1,2]. Multistep deregulation of key transcription factors and genes controlling self-renewal, senescence, apoptosis, differentiation or proliferation in a T-cell precursor leads to clonal transformation and expansion of blast cells in the lymphoid organs and the bone marrow[1,3–7]. Although most T-ALL patients at diagnosis achieve remission with intensive chemotherapy and glucocorticoids, 15% to 40% of the patients subsequently experience relapse into a resistant leukemia with dismal prognosis[8–10]. Therefore, comprehensive understanding of the functional mechanisms underlying relapse and resistance is a major unmet need to develop more efficient therapeutic strategies. While exhaustive genetic and immunophenotypic landscape studies have enabled to identify a large variety of T-ALL subtypes[2,7,11,12], these last only partially correlate with the onset of relapse. It rather appears that resistance initiates upon treatment by the selection of residual T-ALL cells with cellular features driving cell survival despite therapy and allowing re-expansion[13–19]. Selection of *NT5C2* somatic mutations leading

to cell resistance to 6-mercaptopurine is a well-established, although rare, example of resistance-driven mechanism in T- and B-ALL patients[20–24], but alternative mechanisms remain elusive.

Here, we investigated *TP53* alterations (*TP53*^{alt}, i.e. *TP53* somatic mutations and/or deletions) as a factor of resistance acquisition in T-ALL. While rarely detected at diagnosis (2-3%), *TP53*^{alt} are frequently found at relapse (up to 25%) and are associated to poor clinical outcomes[25–30]. *TP53*^{alt} cells are genetically trackable, allowing to detect and characterize them at various stages of T-ALL progression (diagnosis, remission or relapse). Using *in vivo* isogenic patient-derived xenografts (PDX) of diagnosis and relapse T-ALL pairs, we unveiled a unique relapse phenotype that included increased leukemia initiating activity and modulation of key signaling and metabolic pathways such as MYC and OXPHOS. Integration of multi-omics and functional data, including single-cell analyses, allowed us to delineate the relapse trajectory of rare, therapy-selected cells pre-existing at diagnosis that subsequently expanded sequentially and drove relapse.

RESULTS

Isogenic, patient-derived xenografts (PDXs) faithfully capture T-ALL diagnosis and *TP53*^{alt}-driven relapse genomic patterns

We aimed at uncovering functional mechanisms involved in leukemia resistance and relapse. We focused on *TP53*-altered T-ALL since *TP53* alterations are well-recognized, genetically-trackable, drivers of relapse but are still poorly mechanistically understood in T-ALL[25–29,31]. We selected four cases of T-ALL with *TP53* alterations at relapse only for which cryopreserved diagnosis and relapse patient samples were available. To overcome the limitations of *ex vivo* functional studies on primary samples or cell lines, we established PDXs of paired diagnosis (Dx) and relapse (Rel) leukemia in immunodeficient NOD.Cg-*Prkdc*$_{scid}$ *IL2rg*$_{tm1Wjl}$/SzJ (NSG) mice (**Figure 1A**). Genomic analyses of the resulting isogenic, Dx-Rel PDX pairs showed that these PDXs largely captured the genomic pattern of the patient cells, both at diagnosis and at relapse, respectively (**Figure 1B** and **Supplementary Tables 1-2**). *TP53* alterations in patient T-ALL relapse cells were missense mutations in the *TP53* DNA-binding domain within mutational hotspot residues R175 and R248 (cases TALL42; and TALL11 and TALL43, respectively) and a less classical but already reported

114 pathogenic mutation H214 (case TALL30) (**Figure 1C**). The other allele was lost by
115 17p deletion in 3 cases (TALL30, TALL42 and TALL43) or by 17p uniparental disomy
116 of the mutated allele in 1 case (TALL11) (**Figure 1B**). The resulting PDXs carried the
117 original *TP53* missense mutations in association with the loss of the remaining wild-
118 type (WT) allele, as in primary patient samples, or in 1 case only the deleted allele
119 (PDX43R).
120 Interestingly, other somatic copy number variants (CNVs) and point mutations (i.e., in
121 addition to *TP53*^{alt}) were largely similar in both the diagnosis and relapse samples in
122 the T-ALL pairs, suggesting that *TP53*-driven T-ALL relapse did not acquire stronger
123 genomic instability (**Figure 1B**). Therefore, these T-ALL PDX models faithfully
124 captured the diagnosis and the relapse patient samples, respectively, enabling further
125 functional comparison experiments using this unlimited ressources of isogenic, human
126 leukemic cells.
127
128 **Relapse cells display a cell-intrinsic, stable, relapse phenotype compared to**
129 **their isogenic diagnosis cells**
130 To uncover functional mechanisms involved in leukemia resistance and relapse, we
131 compared the leukemia propagation ability of the diagnosis and relapse T-ALL pairs.
132 First, primary leukemic cells from paired Dx-Rel patient samples were transplanted in
133 parallel at equivalent cell doses in NSG mice, and leukemia onset and mice survival
134 were monitored. Despite strong inter-patient T-ALL heterogeneity, we found in each
135 pair that the relapse cells propagated leukemia more efficiently than their diagnosis
136 counterparts (**Supplementary Figure 1A**), which translated into a significantly shorter
137 mice survival (**Figure 2A** and **Supplementary Figure 1B**). This increased leukemia
138 propagating activity at relapse was observed in all PDXs established from the 4 pairs.
139 We performed multiple iterative transplantations using decreasing cell doses (**Figures**
140 **2B-C** and **Supplementary Figures 1C-F**) and found that the propagation phenotype
141 was stable upon serial reinjection, without additional acceleration (**Supplementary**
142 **Figures 1D,1F**). Limiting dilution *in vivo* assays (injection of 10^6 to 1 leukemic
143 cell/mouse) showed that the leukemia initiating cell (LIC) frequencies were increased
144 in the Rel PDXs compared to Dx counterparts (**Figure 2D** and **Supplementary Table**
145 **3**). Consistently, *in vitro* long-term culture-initiating cell assays in coculture with MS5-
146 DL1 stromal cells[32] showed a significantly increased clonogenicity in Rel PDXs from
147 all T-ALL pairs, demonstrating that increased LIC activity is a cell-intrinsic feature of

148 relapse cells (**Supplementary Figure 1G** and **Supplementary Table 3**). Real-time
149 and end-point *in vitro* proliferation using Bromodeoxyuridine (BrdU) pulse labelling and
150 apoptosis experiments, in particular cleaved caspase 3 staining, showed increased
151 proliferation and decreased apoptosis in Rel versus Dx PDX cells (**Figures 2E-F** and
152 **Supplementary Figures 1H-I**). Moreover, homing of the leukemic cells in the bone
153 marrow, spleen and liver at 24 hrs was increased in PDXs from Rel for the 4 T-ALL
154 pairs (**Supplementary Figures 1J-K**). However, when homing was bypassed by direct
155 injection of leukemic cells into the femoral bone marrow cavity, leukemic cells from Rel
156 PDXs still propagated leukemia more efficiently than Dx PDXs (**Supplementary**
157 **Figures 1L-M**).
158 Collectively, our data indicate that despite inter-T-ALL heterogeneity, *TP53*^{alt} mediate
159 a unique, cell-intrinsic, relapse phenotype that is associated with increased
160 proliferation, cell survival, and cell homing and post-homing advantage, resulting in
161 higher LIC activity.
162
163 **Experimental *TP53* silencing confers the cell-intrinsic relapse phenotype to**
164 **diagnosis leukemic cells**
165 To model *TP53* alterations as driver of the relapse phenotype, we inactivated *TP53*
166 using a lentiviral shRNA approach in Dx PDX leukemic cells followed by transplantation
167 in NSG mice (**Figure 3A** and **Supplementary Figure 2A**). *TP53* downregulation
168 increased the leukemia propagation capacities of Dx PDX cells when transplanted
169 under parallel and competitive settings (**Figure 3B** and **Supplementary Figures 2B,**
170 **2D-E**), and resulted in enhanced leukemia spreading and shorter survival of the
171 recipient mice (**Figure 3C** and **Supplementary Figure 2C**). This phenotype was
172 retained in secondary transplants, both in parallel and competitive settings (**Figures**
173 **3D-F** and **Supplementary Figures 2F-H**).
174 *In vitro* long term culture-initiating cell assays and proliferation experiments on the
175 *TP53*-silenced Dx PDX cells confirmed the relapse phenotype, indicating a *TP53*-
176 dependent increased clonogenic activity (**Figure 3G**, **Supplementary Table 3** and
177 **Supplementary Figure 2I**). Finally, *in vivo TP53*-silenced Dx cells also displayed
178 increased homing and post homing capacities (**Supplementary Figures 2J-M**).
179 Altogether, these results demonstrate that *TP53* silencing suffices to confer functional
180 features of the relapse phenotype to patient diagnosis cells.
181

182 ***TP53* alterations deregulate MYC signaling and metabolism pathways in T-ALL**
183 **cells and directly contribute to the *relapse phenotype***
184 To dig into the biological pathways deregulated by *TP53*^{alt} in T-ALL relapse, we
185 compared transcriptional profiles of isogenic Dx and Rel T-ALL PDX samples. While
186 91 genes were upregulated at relapse, 181 genes were downregulated including *TP53*
187 itself (except in PDX11R where *TP53* was point-mutated on both alleles) (**Figure 4A**
188 and **Supplementary Figures 3A-B**). Geneset enrichment analysis (GSEA) identified
189 the MYC, E2F, and G2M checkpoint pathways as enriched in Rel cells along with
190 several cell metabolism pathways, including oxidative phosphorylation (OXPHOS),
191 glycolysis and cholesterol homeostasis, defining a relapse expression signature
192 (**Figure 4B**). Moreover, we interrogated genesets linked to cell proliferation,
193 invasiveness and stemness, and evidenced their upregulation at relapse
194 (**Supplementary Figure 3C**). Analysis in secondary transplant PDXs showed
195 consistent expression patterns, demonstrating functional stability (**Supplementary**
196 **Figures 3D-G**). The relapse expression signature was also retrieved from the
197 corresponding primary T-ALL samples, further outlining that our Dx-Rel PDX models
198 faithfully captured the features of the patient cells (**Figure 4C**).
199 Considering the role of TP53 in regulating MYC signaling and metabolism
200 pathways[33,34], we focused on OXPHOS and glycolysis and performed real-time
201 measurements of oxygen consumption rate (OCR) and extra cellular acidification rate
202 (ECAR) in isogenic Dx-Rel PDX pairs. We found increased basal and maximal
203 mitochondrial respiration, along with increased glycolysis, in the Rel vs Dx T-ALL cells
204 (**Figures 4D-E** and **Supplementary Figures 3H-K**). Consistently, experimental
205 silencing of *TP53* in the diagnosis PDX cells conferred a relapse mitochondrial and
206 glycolytic profile, demonstrating a driver role of *TP53* inactivation into deregulation of
207 metabolic functions (**Figures 4F-G** and **Supplementary Figures 3L-N**).
208
209 **Backtracking pre-relapse *TP53*^{alt} clones at diagnosis**
210 As T-ALL relapse may emerge from minor pre-existing subclones at
211 diagnosis[13,17,19,22,35,36], we next aimed to backtrack rare *TP53*-mutated cells that would
212 constitute a genetically defined pre-relapse reservoir. We performed ultra-sensitive,
213 quantitative, droplet digital PCR (ddPCR) approach on the isogenic Dx-Rel primary
214 and PDX samples. We retrieved the expected *TP53*-associated relapse mutation in
215 the primary and/or PDX sample from diagnosis in 3 out of 4 cases (all but TALL11),

216 with very low variant allele frequencies (VAF) ranging from 0.01 to 0.04% that could
217 be extrapolated to approximately 1/1250 to 1/5000 total cells, i.e., below the usual
218 medical diagnosis detection thresholds of dominant genetic subclones). These results
219 indicate the presence at diagnosis of a very minor *TP53*-mutant clone that was further
220 selected and expanded in the post-treatment relapse sample. Interestingly, a
221 cryopreserved remission sample was also available in case TALL11, in which we
222 detected the expected *TP53*-R248Q mutation with a low frequency (VAF, 0.02%;
223 approximately 1/2500 total cells), demonstrating the existence of the mutant cells
224 reservoir during treatment. When this remission sample was injected into NSG mice,
225 a full-blown leukemia developed from these rare cells. All the resulting leukemic cells
226 carried the *TP53*-R248Q missense mutation. Interestingly, this leukemia retained a
227 wildtype allele (*TP53*-R248Q allele frequency, 46% in sorted leukemic cells),
228 contrasting with the relapse cells that demonstrated copy-neutral loss of the wildtype
229 allele (*TP53*-R248Q allele frequency, 92%). This highlights the selective advantage
230 upon treatment conferred by the monoallelic point mutation to a minor clone at
231 remission, which further expanded in the PDX. The relapse cells displayed a complete
232 loss of the wildtype *TP53* allele and function with duplication of the *TP53*-R248Q allele
233 through acquisition of an uniparental disomy.
234 Those data demonstrate that relapse emerged from a pre-existing ultra-minor *TP53*-
235 mutant clone that expanded during treatment through selective growth advantage, and
236 subsequent acquisition of bi-allelic *TP53* loss at full relapse.
237
238 **Combined single-cell profiling uncovers pre-relapse, reservoir cells at diagnosis**
239 **that express features of the relapse phenotype**
240 To further evaluate whether the rare *TP53*-mutant population from diagnosis
241 expressed a relapse-like transcriptional state, we performed single-cell RNAseq
242 analysis on the 4 T-ALL pairs. The 16 resulting samples (8 primary and 8 from PDXs)
243 did not globally cluster by their diagnosis or relapse nature (i.e., all diagnosis *versus*
244 all relapse samples), nor by their origin (i.e., all primary *versus* all PDX samples), or by
245 cell cycle repartition, but rather by individual T-ALL case (**Figure 5A** and
246 **Supplementary Figures 4A-B**), underlying prominent inter T-ALL biological
247 heterogeneity. GSEA confirmed oxidative phosphorylation signature as the most
248 differentially expressed pathway in all relapse samples along with cell proliferation, cell

signaling and cell metabolism pathways (**Supplementary Figures 4C-F** and **Figures 5B-C**).

Comparison of the diagnosis and relapse samples uncovered a minor cell population in two diagnosis samples (TALL42 and TALL30) that clustered nearby their paired relapse counterparts, suggesting the existence of a “pre-relapse” cells transcriptional state at diagnosis (**Supplementary Figures 4C, 4E**). We further integrated the combined analyses of mutation, copy number and TCR rearrangement to reconstitute leukemia architecture before and after treatment along with single-cell expression profiling in these two cases (**Figure 5D**).

In case TALL42, the small cluster of cells represented approximately 10% of the total leukemic cells at diagnosis (9.6% and 15% of the primary and PDX samples, respectively) (**Figures 5E-F** and **Supplementary Figures 4G-Q**). This minor cell population displayed both a distinct TCRB rearrangement (TCRB#2) and a distinct second-allele 9p/*CDKN2A* deletion from the dominant clone at diagnosis, and no 17p deletion, while the relapse population displayed the same subclonal TCRB#2 but yet another 9p/*CDKN2A* deletion (specific to relapse) and both the *TP53*-R175H and del17p/*TP53* (those last being not detected by NGS and inference analysis in the 10% subclone at diagnosis) (**Figure 5D** and **Supplementary Figures 4I, 4K, 4P, 4R**). Interestingly, the minor subpopulation at diagnosis was enriched in most of the relapse expression signature including OXPHOS, MTORC1 signalling, MYC targets V1, E2F targets, cholesterol homeostasis and DNA repair, these pathways being even more upregulated in the matched relapse cells (**Figure 5G** and **Supplementary Figure 4S**). We interrogated additional geneset collections and found a significant enrichment of stemness, invasiveness and OXPHOS signatures combined with downregulation of cell proliferation pathways, in line with the properties attributed to a quiescent, LIC-activity enriched, pre-relapse leukemia reservoir (**Figure 5H** and **Supplementary Figure 4T**). Specifically, interrogation of several leukemia stem cell (LSC) signatures[37–40] showed that this cluster had increased LSC signature scores compared to diagnosis cells, as in relapse cells (**Figure 5I**).

In the second case, TALL30, a minor cell population representing approximately 5% at diagnosis, trackable by the same TCRB rearrangement as relapse cells but distinct from the dominant diagnostic population, also demonstrated the deregulation of the relapse signature (**Supplementary Figure 5**).

282 Clearly, the very low frequency of the *TP53* mutation in the two cases (VAF <0.02%
283 as found by ddPCR) contrasted with the 5-10% frequency of the minor cell population
284 expressing the relapse signature. In case TALL42, the clonal architecture showed that
285 both the 5-10% minor clone population and the *TP53*^{alt} mutation derived from a
286 common ancestor bearing the same TCRB rearrangement from which they diverged
287 by acquiring a distinct 9p/*CDKN2A* second-allele deletion in addition to the *TP53*
288 mutation in the relapse clone (**Figure 5D**). In case TALL30, the *TP53*-mutated cells
289 may have emerged from the minor cell population or from an ancestor pre-relapse
290 reservoir. Although somewhat counterintuitive, these data suggest that relapse may
291 be primed in a pre-existing reservoir population expressing the relapse expression
292 signature, the *TP53* mutation occurring in a fraction of those cells that further expand
293 upon treatment. To investigate this hypothesis, we performed deep-sequencing, long-
294 read Nanopore scRNAseq on the 10X cDNAs to track the *TP53* mutations at the single-
295 cell resolution, allowing to directly assess the transcriptional profile of the very rare
296 *TP53*-mutant cells. In TALL42, we obtained a final mean depth of 110X at diagnosis
297 and 40X at relapse, in 8.861 cells and 6.022 cells respectively. The expected *TP53*-
298 R175H missense mutation was retrieved in all (35/35) covered reads from the del17p
299 relapse sample, but also in rare (6/193) reads from the diagnosis sample (**Figures 5J-**
300 **L** and **Supplementary Figures 4U-V**). While not directly numerically comparable to
301 ddPCR since they operate at different biological and technical levels (allele level
302 quantification versus transcriptional profiling), these data confirmed the enrichment of
303 the relapse expression signature in the rare *TP53*-mutated cells as compared to the
304 vast majority of *TP53 WT* cells from diagnosis (**Figure 5M**). Similar results were
305 obtained in the second TALL30 case in which the relapse expression signature was
306 also enriched in the rare *TP53*-mutant cells detected at diagnosis (**Supplementary**
307 **Figures 5P-U**).
308 Collectively, our data show that *TP53*-mutated cells pre-existing at diagnosis
309 constituted a pre-relapse reservoir population expressing the relapse signature, that
310 expanded upon treatment along with sequential inactivation of the second *TP53* allele.
311
312
313 **DISCUSSION**
314 Treatment failure and subsequent patient death for ALL are largely related to the
315 emergence, within the first 2-years, of a relapse much less responsive to therapies

316 than the initial diagnosis leukemia. Comprehensive longitudinal genomic studies on
317 patient cohorts showed that rather than being subtype dependent, resistance initiates
318 upon treatment by the selection of residual, ancestor T-ALL cells surviving therapy and
319 re-expanding[13–19]. However, no clear genomic driver of relapse were detected in most
320 cases and the underlying mechanisms, possibly non-genetic, remain elusive. Here, we
321 leveraged *TP53*^{alt} T-ALL relapse cases, i.e. leukemia with a clear, genetically-trackable
322 driver of resistance to develop faithfull *in vivo* models, based on isogenic diagnosis-
323 relapse paired xenografts, and analysed cellular features driving cell survival and re-
324 expansion. Contrasting with many other T-ALL cases where we previously shown that
325 the PDX resulting from diagnosis more closely resembled relapse samples than bulk
326 diagnosis samples[13], diagnosis and relapse features were faithfully captured in these
327 isogenic PDX pairs resulting from *TP53*^{alt} T-ALL. This substantial difference may be
328 due to the *TP53* lesions nature confering an *in vivo* advantage upon treatment only, as
329 seen in other premalignant conditions[18,41]. Importantly, these isogenic PDX models
330 enable to overcome fundamental limitations of *ex vivo* functional studies on primary
331 samples or cell lines, i.e. rarity and practical workability for primary samples; highly
332 rearranged and drifted cells for cell lines; and, more generally, a lack of
333 microenvironnement support. In addition, isogenic PDXs also allow to avoid bias
334 related to inter-patient heterogeneity, such as the markedly distinct proliferation range
335 between our four T-ALL cases, faithfully captured by the isogenic PDX pairs
336 (**Supplementary Figure 1B**).
337 Interestingly, we found that the *TP53*^{alt}-driven T-ALL relapse cells did not display strong
338 genomic instability, suggesting a direct oncogenic role of *TP53* alterations in those
339 leukemias as “gatekeeper” rather than its commonly recognized “caretaker” role. This
340 was confirmed by *TP53* silencing experiments evidencing a cell-intrinsic gain of
341 malignancy in relapse cells largely driven by the *TP53* inactivation itself. The relapse
342 phenotype we identified includes a cell-intrinsic functional gain of LIC and proliferation,
343 along with an expression profile that involved cell metabolism, signaling, MYC
344 pathways, and stemness, consistently with a role of *TP53* in the regulation of normal
345 and pathologic stem cell function in hematopoiesis[42]. We especially evidenced
346 functionally that increased *TP53*^{alt}-dependent OXPHOS was crucial to the relapse
347 phenotype, as may be seen in other acute leukemia subtypes such as acute myeloid
348 leukemia or various solid cancers[43,44].

349 By combining single-cell transcriptomics, genomics and ultra-sensitive specific
350 backtracking by ddPCR at diagnosis, we could reconstitute the clonal architecture at
351 diagnosis and relapse in two cases (**Figure 5D**). We detected the expected *TP53*
352 mutations at diagnosis at ultra-low frequencies, showing that the relapse originated
353 from a pre-existing ultra-rare reservoir. Interestingly, a remission sample from one case
354 could be injected and expanded towards an overt T-ALL PDX that was *TP53*-
355 mutatedbut not yet 17p deleted, demonstrating the sequential bi-allelic acquisition
356 through leukemia progression. Intriguingly, a transcriptional cluster representing a cell
357 population of approximately 5-10% of cells was detected in two cases at diagnosis,
358 although the vast majority of those cells were *TP53*^{WT}. In one of these two cases
359 (TALL42), clonal architecture demonstrated that a rare *TP53*-mutated clone and the
360 minor (5-10%) cell population issued from the same ancestor, distinct from the
361 dominant clone at diagnosis. In the second case, the *TP53*-mutation may have
362 emerged directly from the minor cell population expressing the relapse signature or
363 from an ancestor. These data raise the possibility that the *TP53* mutation would
364 stabilize a pre-existing transcriptional state, possibly non genetically-driven. Taken the
365 similarity of the relapse signature and the effects of *TP53* inactivation, this minor
366 population may exhibit transcriptional features associated with the relapse because of
367 a functional, rather than genetic, inactivation of TP53 signaling. Beyond the *TP53*-
368 associated relapses we explored in this study, many T-ALL relapses do not display
369 any additional "relapse-associated genes"[17], suggesting that leukemia resistance and
370 relapse might be driven by non-genetic mechanisms. In line with this observation,
371 several studies have raised a spectrum of key epigenetic, transcriptionnal remodeling,
372 cell plasticity and microenvironmental mechanisms that may contribute to
373 relapse[17,35,37,40,48,49]. It will thus be of interest to study whether the *TP53*^{alt}-driven
374 relapse phenotype we identified here can also be relevant in T-ALL cases lacking *TP53*
375 genetic alterations at relapse, suggesting non-genetic driver mechanisms.
376 Like in the vast majority of cancers, *TP53*^{alt} T-ALL relapses are associated with very
377 poor clinical outcomes and limited therapeutic options, representing a major clinical
378 challenge. Detecting very rare pre-existing *TP53*-mutant cells at diagnosis, i.e., below
379 usual thresholds, potentially combined with single-cell transcriptomic detecting high-
380 risk cellular state, and *TP53*^{alt} bi-allelic deletion tracking, may be of broad interest for
381 patient monitoring and early intervention with targeted therapies or hematopoietic stem
382 cell transplantation.

383
384
385
386
387
388 **METHODS**

389 **Patient cohort, collection of biological material and annotations.** Primary samples
390 from 42 T-ALL patients who have relapsed were obtained from blood or bone marrow
391 (BM) aspirates/biopsies at initial diagnosis, remission (non tumoral, considered as
392 germline reference) and first relapse. The cohort included children and young adults
393 (age, 1 to 42 years old). Samples were stored in the Tumor Bank of Saint-Louis
394 Hospital, Paris (BiRTH, Biobank for Research in Translational Hematology)
395 accordingly to the French law, including informed consent. Annotations of T-ALL
396 mutations were obtained using the NGS sequencing and analysis pipeline from Saint-
397 Louis Hospital, using a VAF threshold of 2%[50]. Seven of the 42 patients (16.7%) had
398 *TP53* alterations at relapse, including 4 for which live cells from both diagnosis and
399 relapse could be recovered and injected to mice. IRB approval from the Inserm was
400 given to this study under the number #12–078.
401

402 **Animal studies.** Mice experiments described in this study comply with the current
403 ethical regulations. Authorizations for animal experimentation were obtained from the
404 *Ministère de l'enseignement supérieur et de la recherche* with the No. APAFIS#19958-
405 2019032615074625v2 and APAFIS#47448-2024020909144467v3. Mice were housed
406 under a dark-light cycle at ambient temperature (≈20-24°C) with a humidity of 40-60%
407 and handled in a pathogen-free animal facility in accordance with the guidelines of the
408 Animal Care and Use Committee (IRSL, Université Paris Cité). Animals were excluded
409 from experiments if any sign of stress were observed without clinical signs of full-blown
410 leukemia development (i.e. absence of human leukemic cells in blood, bone marrow
411 and spleen).
412

413 **Patient derived xenografts (PDXs) of isogenic diagnosis-relapse T-ALL samples.**
414 Isogenic diagnosis (Dx) and relapse (Rel) T-ALL patient samples were thawed,
415 qualified and injected intravenously (unless otherwise stated) at equivalent cell doses
416 into sublethally irradiated immunodeficient NOD.Cg-Prkdc$_{scid}$ IL2rg$_{tm1Wjl}$/SzJ (NSG)

417 mice from the Jackson Laboratory that are bred locally, as described previously[50].
418 Leukemia development was monitored monthly by flow cytometry (FACS) analysis of
419 blood or BM aspirates using hCD45 and hCD7-based staining protocol detailed in the
420 'Flow cytometry' section to confirm disease engraftment.
421 Human T-ALL cells from both patients and derived PDXs (BM of fully leukemic mice
422 with >95% blasts) were used for genomics, molecular and functional experiments. To
423 evaluate the stability of the phenotype from PDX models, leukemic cells from PDXs at
424 first passage were serially transplanted into NSG recipient mice by intravenous
425 injection (unless otherwise stated) at equivalent cell doses. In some circumstances to
426 evaluate post homing involvement, leukemic cells from isogenic Dx-Rel PDXs were
427 injected into sublethally irradiated mice by intrafemoral route. Recipient mice were
428 monitored daily by visual and clinical observations and monthly for biological
429 parameters, i.e. signs of stress (weakness, weight loss, ruffled coat, lethargy or ataxia)
430 and the presence of human leukemic cells in blood and/or BM. To monitor survival,
431 mice were sacrificed at or before reaching ethical endpoints. Pathology and flow
432 cytometry analyses confirmed full-blown T-ALL disease with marrow, spleen and liver
433 infiltration by leukemic cells.
434
435 **Flow cytometry.** Leukemic cells obtained from peripheral blood after Ficoll separation
436 and from BM aspirates were washed and resuspended in PBS (*Gibco*) supplemented
437 with 2% FBS (*Gibco*) before staining. Human leukemic cells infiltration in NSG recipient
438 mice was measured in legs, spleen and liver that were crushed or mashed. Leukemic
439 cells suspensions were washed and resuspended in PBS supplemented with 2% FBS
440 for staining. Human leukemic cells were then stained for 30 min at 4°C with anti-human
441 CD45 (APC or VioBlue) and CD7 (PE or PE-Vio770) antibodies (*Miltenyi Biotec*) (1:100
442 dilution). Cells were then washed and analysed on a FACS Canto II or LSR Fortessa
443 analyzer (*BD Biosciences*). Flow cytometry analyses were performed using Flowjo
444 10.10 (*TreeStar*).
445
446 **Whole Exome Sequencing Analysis of primary and PDX T-ALL samples.** Primary
447 samples from matched tumoral (initial diagnosis and first relapse) and non-tumoral
448 (remission) obtained from T-ALL patients and the corresponding isogenic Dx-Rel PDXs
449 were subjected to deep whole-exome sequencing (WES). DNA libraries were prepared
450 using SureSelect XT Target Enrichment according to the manufacturer's instructions

451 (*Agilent Technologies*, Santa Clara, CA, USA). Exon capture was performed with
452 Agilent SureSelect Human All Exon V5 kit. The samples were sequenced on an
453 Illumina NextSeq 500 platform (*Illumina*, San Diego, CA, USA) in a 2 × 100 bp paired-
454 end sequencing run. The average sequencing depth was 110X. Raw data were first
455 submitted to quality check using Trim_Galore (v0.6.6) to perform quality and adapter
456 trimming for paired-end reads. The paired end clean reads were aligned to the human
457 reference genome (hg19) using BWA (v0.7.17-r1188). Duplicates reads were flagged
458 using Picard-tools (v2.3.0) and local realignment around InDels and base quality score
459 recalibration was performed using Genome Analysis ToolKit (GATK v4.2.5.0).
460 Somatic mutations were called by VarScan somatic (v2.4.2) and annotated by
461 ANNOVAR (version 2022-04-13) before filtering. Somatic copy number variants
462 (CNVs) were detected by facets (v0.16.0-1) and by an in-house R script. The final
463 retained abnormalities were validated by visual inspection considering a number of
464 markers ≥2 and log2ratio with respect to the individual background noise.
465 Exon capture was performed with Agilent SureSelect Human All Exon V6 UTR kit for
466 the isogenic Dx-Rel PDX pairs. The same procedure as above was used to analyse
467 PDX samples (n= 8) using the corresponding primary non-tumour sample as reference
468 for somatic calling variant step. The overlap between V5 and V6_UTR capture was
469 performed for the upstream analysis.
470
471 ***In vivo* limiting dilution experiments.** Leukemic cells from paired Dx-Rel PDXs
472 (primografts) were intravenously injected under limiting dilution conditions from 10^6 to
473 1 cell per sublethally irradiated mouse (up to 6 mice per condition). Leukemia
474 development in recipient NSG mice was monitored monthly by blood or BM aspirates.
475 All mice were sacrificed at or before reaching ethical endpoints. Blast infiltration was
476 confirmed as detailed above. Pathology analysis confirmed full-blown T-ALL diagnosis,
477 with BM, spleen and liver infiltration by lymphoblasts expressing human CD45 and
478 CD7 markers. Leukemia initiating cell (LIC) frequencies of isogenic Dx-Rel T-ALL
479 PDXs were calculated from the number of engrafted mice for each cell dose in each
480 condition using the WEHI bioinformatic ELDA (Extreme Limiting Dilution Analysis)
481 software[51]. *P* values were calculated with overall tests for differences in LIC
482 frequencies between any of the group tested.
483

484 ***In vitro long term culture-initiating cell* experiment.** Leukemic cells from isogenic
485 Dx-Rel T-ALL PDX samples (primografts) and from paired control mCherry$^+$ and *TP53*
486 KD GFP$^+$ PDX samples at diagnosis were sorted by flow cytometry based on
487 CD45$^+$CD7$^+$ (+/- GFP$^+$ or mCherry$^+$) and seeded on irradiated (30 Gy) confluent
488 stromal cells under limiting dilution conditions from 78.125 to 1 cell per well (24 wells
489 per condition). Leukemic cells were then cocultured on stromal feeder cells for 2 to 4
490 weeks under hypoxic condition (3% O_2) as previously described[50]. Cell medium was
491 partially changed twice a week. Positive wells for leukemic cells outgrowth were
492 visually scored at regular time intervals. Leukemic cells detection was confirmed by
493 flow cytometry analysis of recovered wells after 2 to 4 weeks of culture upon hypoxia
494 as detailed above to confirm the presence of leukemic cells. LIC frequencies were
495 calculated from the number of positive wells for leukemic cells outgrowth for each cell
496 dose in each condition using the WEHI bioinformatic ELDA software[51]. *P* values were
497 calculated with overall tests for differences in LIC frequencies between any of the group
498 tested.
499
500 **Real-time measurement of leukemic cells proliferation and apoptosis with the**
501 **IncuCyte® Live-Cell Analysis System.** Real-time measurement of *in vitro* leukemic
502 cell proliferation and apoptosis was performed using the IncuCyte® Live-Cell Analysis
503 System (*Sartorius*). Human CD45$^+$CD7$^+$ leukemic cells from isogenic Dx-Rel T-ALL
504 PDX samples (primografts) were sorted by flow cytometry and 100.000 cells were
505 seeded on 96-well flat bottom plate (4 wells per condition) previously coated with 0.4μg
506 of purified human Delta4-Fc fusion protein (*PX'Therapeutics*) according to
507 manufacturer's recommendation. Leukemic cells were cultured as previously
508 described[50] for up to 96 hours under normoxia in the IncuCyte® system (5% CO_2 and
509 37 °C). Real-time *in vitro* leukemic cell growth was monitored using live-cell time-lapse
510 imaging by capturing phase contrast images every 2 hours and analysed using the
511 integrated confluence algorithm provided. Cell proliferation was represented as the
512 proportion of phase objects confluence over time, without labels. Leukemic cell
513 apoptosis was detected using the IncuCyte® Caspase-3/7 green reagent for apoptosis
514 (*Sartorius*). Briefly, leukemic cells were cultured as previously described in the
515 presence of 5μM Caspase-3/7 green reagent. Real-time live-cell imaging of apoptosis
516 was monitored by capturing phase contrast and green fluorescence images every 2
517 hours and analysed using the integrated algorithm provided. Leukemic cell apoptosis

518 was represented as the proprotion of green fluorescently labelled nuclei after activated
519 caspase-3/7 cleavage of inert Incucyte® Caspase-3/7 dye.
520
521 **Apoptosis and cell proliferation end-point assays.** Leukemic cells from isogenic
522 Dx-Rel PDX T-ALL samples were co-cultured on stromal cells[50] for 48 hours under
523 normoxia in a humidified 5% CO_2 incubator at 37°C. To perform apoptosis assay,
524 leukemic cells from co-cultures were then collected, washed and stained as detailed
525 above. Leukemic cells were then fixed and stained with PE or Biotin anti-Cleaved
526 Caspase 3 antibody (*BD Biosciences*) as recommended by the manufacturer's
527 recommendations, washed and then analyzed by flow cytometry on FACS Canto II or
528 a LSR Fortessa analyzers (*BD Biosciences*). Cell cycle assays were performed using
529 the APC BrdU Flow kit (*BD Pharmigen*) as recommended by the manufacturer's
530 recommendations. Briefly, leukemic cells co-cultured on stromal cells for 48 hours
531 were pulse-labeled for one hour at 37°C with 1mM Bromodeoxyuridine (BrdU).
532 Leukemic cells from the recovered co-cultures were stained with cell surface
533 antibodies as above. Leukemic cells were then fixed, permeabilized, incubated with
534 DNase and stained with APC-conjugated anti-BrdU antibody (1:100 dilution) for 20 min
535 at room temperature and incubated with Vybrant violet (1:1000 dilution, *Invitrogen*) for
536 30 min at 37°C before FACS analyses.
537
538 ***In vivo* homing assay.** Leukemic cells from isogenic Dx-Rel PDXs or from matched
539 *TP53*KD and controls Dx PDXs were injected intravenously (2-6x10^6 cells/mouse) into
540 sublethally irradiated immunodeficient NSG recipient mice (n = 2 to 4 mice per group).
541 Homing capacities of human leukemic cells were evaluated 24 hours after intravenous
542 injection by FACS analysis of BM, spleen and liver.
543
544 ***TP53* gene silencing in human leukemic cells and *in vivo* transplantations.** The
545 Hu ShRNA anti-*TP53* was previously described[52]. The human *TP53* cDNA was cloned
546 under the H1 promoter in the backbone pRRL.SIN.cPPT.PGK.GFP lentiviral vector
547 (*Addgene* plasmid #22038). The pRRL_H1shCTL_PGK_mCherry lentivector was
548 constructed in house from the pRRL_H1shLacZ_PGK_eGFP mentioned above.
549 Lentiviral particles were produced as described[53] with jetPRIME reagents (*Polyplus*
550 *transfection*) by co-transfection of viral production plasmids, according to the
551 manufacturer's protocol. Lentiviral supernatants titration was performed using the

552 qPCR Lentivirus Titer Kit (*Applied Biological Materials*) according to the manufacturer's
553 recommendation.
554 Leukemic cells from primary PDX samples at diagnosis were cultured on 24-wells
555 plates previously coated with 2.5μg of purified human Delta4-Fc fusion protein
556 (*PX'Therapeutics*) and transduced for 48-72 hours with the lentiviral supernatants
557 including controls (at MOI 20-50) in the presence of 4ug/ml Protamine sulfate (*Sigma*).
558 Transduced leukemic cells were then washed , GFP- and mCherry-FACS sorted and
559 immediately intravenously injected into sub-lethally irradiated NSG mice, at equivalent
560 dose in parallel settings. For competitive experiments, leukemic cells transduced with
561 a shRNA CTL mCherry or shRNA *TP53*-GFP lentivirus were FACS-sorted, and mixed
562 in equivalent number before intravenous injection into sub-lethally irradiated NSG
563 mice. The starting GFP^+/$mCherry^+$ ratio was re-checked by flow cytometry before IV-
564 injection. Gene silencing efficiency was checked by immunoblot (human p53 D0-1,
565 *Santa Cruz*; Actin,*Santa Cruz*).
566
567 **Large-scale gene expression analysis of primary and PDX T-ALL samples by**
568 **bulk RNA sequencing analysis.** Total RNAs were extracted from frozen pellets of
569 leukemic blasts at initial diagnosis and first relapse (n= 8 samples) and from BM of fully
570 leukemic NSG mice for the corresponding derived PDXs (n= 24 PDX samples, first
571 injection) using Qiagen RNA extraction kit (*Qiagen,* miRNeasy Tissue cell advance)
572 according to the manufacturer's recommendations. cDNA libraries were prepared
573 using the TruSeq Stranded mRNA kit (*Illumina*, San Diego, CA, USA). Alignment to
574 the hg19 (GRCh37) reference genome was performed using STAR aligner (Version
575 2.7.8a) with quantMode GeneCounts parameter to build raw count matrix for gene-
576 level summarisation based on the in-built hg19 RefSeq-based annotation.
577 Normalisation by the method of trimmed mean of M-values (TMM) was performed
578 using the calcNormFactors function in edgeR. A linear model fitted in limma package
579 was performed to identify differential gene expression between relapse and diagnosis
580 samples in basal conditions. Differentially expressed genes were identified based on
581 the adjusted *p*-value < 0.05 and filtered with a fold change absolute value > 0.5. The
582 relationship between samples was visualized by hierarchical clustering and principal
583 component analysis (PCA). Over Representation Analysis (ORA) and Gene set
584 enrichment analyses (GSEA) were then performed to identify significant - hallmark,
585 positional (C1), curated (C2), and ontology (C5) - genes sets using the fgsea and

586 msigdbr packages. Additional analyses on PDX samples from secondary transplants
587 were performed using the ClariomTM D Assay plateform (*Thermo Fisher Scientific*)
588 using the manufacturer's recommendations.
589
590 **Mitochondrial Respiration and Glycolytic Function Measurements.** Oxygen
591 consumption rate (OCR) and extracellular acidification rate (ECAR) were respectively
592 measured with the Seahorse XFp Cell Mito Stress and XFp Glycolysis Stress Test kits
593 on the Seahorse XFp Analyser (*Agilent, Seahorse Bioscience*) in accordance with the
594 manufacturer's recommendations. Leukemic cells recovered from 24h co-culture on
595 stromal cells were seeded at 4 x 10^5 cells per well (optimal cell seeding density was
596 determined in preliminary experiments) in an XFp-well miniplate previously coated with
597 Cell-Tak (*Corning, Fisher Scientific*) in 180µl of XF DMEM Medium (pH 7.4),
598 supplemented with 2 mM L-glutamine (*Gibco*) (for OCR and ECAR), 1 mM fresh
599 sodium pyruvate (*Gibco*) (for OCR only) and 10 mM D-glucose (*Sigma*) (for OCR only)
600 on the day of the assay. For OCR measurements, sequential compound injections of
601 Oligomycin (1µM), FCCP (1µM), Rotenone (0.5 µM) and Antimycin A (0.5µM) enabled
602 measurements of basal respiration, ATP production, proton leak, maximal respiration,
603 spare respiratory capacity, and non-mitochondrial respiration. For ECAR
604 measurements, sequential compound injections of Glucose (10mM), Oligomycin (1µM)
605 and 2-Deoxy-glucose (2-DG, 50mM) enabled measurements of glycolysis, glycolytic
606 capacity, glycolytic reserve and non-glycolytic acidification. Key parameters of
607 mitochondrial respiration and glycolytic functions were recorded for 90 minutes after
608 cells were placed into the analyzer. OCR (pmol/min) and ECAR (mpH/min) were
609 measured simultaneously in all wells, three times at each step, by optical fluorescent
610 O2 sensors, and a minimum of three replicates were analyzed per condition in any
611 given experiment. Unless otherwise stated, all compounds and material were obtained
612 from *Agilent Seahorse Bioscience*.
613
614 **Cell lines and human T-ALL cells culture.** HEK-293T cell line was purchased from
615 ATCC (CRL-3216). HEK-293T cells were grown in DMEM medium (*Gibco*)
616 supplemented with 2mM L-glutamine (*Gibco*), 1% penicillin/streptomycin (*Gibco*), and
617 10% heat-inactivated fetal bovine serum (FBS) (*Gibco*). Mouse MS5-Delta-like1[13,54]
618 and human hTERT-immortalized primary bone marrow MSCs[55] derived stromal cells
619 were maintained in αMEM medium (*Gibco*) supplemented with 2mM L-glutamine

620 (*Gibco*), 1% penicillin/streptomycin (*Gibco*), 1μM Hydrocortisone (*Sigma*, for MSCs
621 only) and 10% heat-inactivated FBS (*Gibco*). All cell lines were grown in a humidified
622 5% CO_2 incubator at 37 °C and tested monthly negative for Mycoplasma using
623 MycoAlert PLUS Mycoplasma Detection Kit (*Lonza,*) or MycoStrip Mycoplasma
624 Detection Kit (*Invivogen*).
625 Primary and PDX human T-ALL leukemic cells were cocultured on stromal cells (MS5-
626 DL1 or hMSC cells) in αMEM medium (*Gibco*) supplemented with 2mM L-glutamine
627 (*Gibco*), 1% penicillin/streptomycin (*Gibco*), 10% heat-inactivated FBS (*Stem Cell*
628 *Technologies*), 10% heat-inactivated human AB serum (*Institut de Biotechnologies*
629 *Jacques Boy*), 20nM Human Recombinant Insuline (*SAFC Sigma*), 50ng/ml Human
630 Recombinant SCF (*Miltenyi Biotec*), 10ng/ml Human Recombinant IL7 (*Miltenyi*
631 *Biotec*), 20ng/ml Human Recombinant Flt3 ligand (*Miltenyi Biotec*) as already
632 described[13,50].
633
634 ***TP53*-mutant cells backtracking in isogenic primary and PDX T-ALL samples by**
635 **droplet-digital PCR.**
636 Droplet-digital PCR (ddPCR) reactions were performed following Bio-Rad
637 recommendation's with 2X ddPCR SuperMix for probes No dUTP and commercially
638 designed ddPCR Mutation Assays for each *TP53* mutation (*Bio-Rad*). Mutation assays
639 are a mix of two fluorescent probes in competition for the annealing on the same target
640 sequence: one specific probe for the wild-type sequence (FAM probe) and a HEX
641 probe, specific of the mutated sequence. Two wet-lab validated ddPCR MUT FAMHEX
642 Assay were used for detection of patient's specific mutations (*TP53*-R175H (Assay ID
643 dHsaMDV2010105) and *TP53*-R248Q (Assay ID dHsaMDV2010127)) and a non-wet-
644 lab validated assay IS ddPCR MUT FAMHEX Assay was used for *TP53*-H214R
645 mutation detection (Assay ID dHsaMDS2510824). Experiments were performed on
646 genomic DNA from isogenic primary and PDX T-ALL samples. Several wells were
647 loaded with DNA from each sample to test enough material. Droplets were generated
648 using QX200 Droplet Generator (*Bio-Rad*). PCR reactions were performed on an
649 Eppendorf Nexus Gradient thermocycler following cycling conditions after validation of
650 optimum annealing/extension temperature: 95°C for 10 min, 40 cycles of two steps
651 PCR 94°C for 30 sec, 55°C for 1 min with a 2°C/sec ramping, an enzyme denaturation
652 step at 98°C for 10 min and a final hold at 4°C. FAM and HEX fluorescence's of each
653 droplet were then read on the QX200 Droplet reader. Visualization, analysis and VAFs

654 calculation were performed with QXOne Manager 1.2 Standard edition software (*Bio-*
655 *Rad*). Thresholds for each assay were determined aiming maximum specificity, despite
656 sensitivity and quantification accuracy by only incorporated double-positive droplets of
657 a well when at least a single positive-droplet was spotted to avoid potential false
658 double-negative droplets (none as "rain droplets") in the analysis. Non-template
659 controls containing all reagents and the corresponding amount of carrier DNA to be
660 equivalent to the tested samples were included in the analysis. VAFs were calculated
661 by considering all the wells analysed.
662
663 **High-throughput short read single-cell RNA sequencing analysis of paired Dx-**
664 **Rel primary and PDX T-ALL samples.** Single-cell RNA-sequencing (scRNAseq)
665 studies were performed on viable leukemic cells prepared from cryopreserved BM
666 samples from T-ALL patients and the corresponding derived PDXs. Libraries from
667 10.000 leukemic cells were prepared using the Chromium Next GEM Single Cell 3'
668 v3.1 reagent kits (*10x Genomics*) and subjected to short read sequencing on the
669 Illumina NovaSeq 6000 platform (*Illumina*, San Diego, CA, USA) in a 28-8-91 paired-
670 end sequencing run (50.000 reads per cell) allowing the captured expression of ~2000
671 genes per cell. FASTQ files were aligned to the human reference sequence (hg38)
672 using CellRanger count pipeline (*10× Genomics*, v3.1.0). The output gene-barcode
673 matrices were imported into the Seurat R package (v4.3.0) for scRNAseq data analysis
674 and visualization. Cells with nFeature_RNA <500 or >20% mitochondrial genes
675 content were filtered out. After removing of low-quality cells, data were normalized
676 using the Normalized-Data function with "LogNormalize" and a scale factor of 10,000.
677 Highly variable features were identified using the FindVariableFeatures function with
678 selection method "vst". Data were scaled using the ScaleData function and S.Score
679 and G2M.Score obtained from CellCycleScoring function were regressed out. Cells
680 were clustered using FindNeighbors (dims =1:50) with the FindClusters function
681 (resolution =0.6) based on the shared nearest neighbour. Datasets were visualized
682 through non-linear dimensional reduction using the Uniform Manifold Approximation
683 and Projection (UMAP). To identify a list of differentially expressed genes, gene
684 expression comparisons between clusters and/or samples were performed using the
685 fast Wilcoxon rank-sum test and area under the receiver operating characteristic curve
686 (auROC) analysis implemented in the R package Presto (v1.0.0). Gene signature
687 scores were computed using the AddModuleScore_UCell function from the UCell R

688 package (v2.6.2), which applies a rank-based scoring method for robust and scalable
689 analysis. To detect large-scale copy number variations in tumor cells, we utilized the
690 inferCNV package (v1.20.0)[56,57]. Gene expression profiles of all relapse cells, or of a
691 defined subset representing the pre-relapse subclone, were contrasted against
692 diagnostic cells to infer chromosomal variations in tumor cell clusters by analyzing
693 expression intensities across genomic locations and thereby explore potential
694 chromosomal alterations.
695
696 **3' single-cell long read sequencing on isogenic Dx-Rel primary T-ALL samples.**
697 Single-cell suspension was converted into barcoded single cell double strand cDNAs
698 using the Next GEM Single Cell 3' Kit (*10X Genomics*, V3.1), aiming for 10,000 cells
699 following the manufacturer's instructions. 10 ng of cDNA amplicons prepared using
700 Next GEM Single Cell 3'Kits (*10X Genomics*, V3.1) were tagged with biotin using PCR
701 amplification following the Oxford Nanopore Technologies (ONT) manufacturer's
702 instructions (SST_9198_v114_revK_29Jan2025) with custom-ordered oligos.
703 [Btn]Fwd_3580_partial_read1_defined_for_3'_cDNA at 10 µM:
704 5'/5Biosg/CAGCACTTGCCTGTCGCTCTATCTTCCTACACGACGCTCTTCCGATCT-
705 3'
706 Rev_PR2_partial_TSO_defined_for_3'_cDNA at 10 µM:
707 5'-CAGCTTTCTGTTGGTGCTGATATTGCAAGCAGTGGTATCAACGCAGAG-3' and
708 LongAmp Hot Start Taq 2X Master Mix (*NEB*).
709 Pull-down of the amplicons on M280 streptavidin beads (10 µg/µl, *Invitrogen*) was
710 performed before a second PCR using the PCR Primers (PRM) included in the PCR
711 Expansion kit (EXP-PCA001) and LongAmp Hot Start Taq 2X Master Mix (*NEB*). A
712 standard Ligation Sequencing Kit V14 library preparation (SQK-LSK114) was
713 completed to prepare the cDNA ends for sequencing on a PromethION device. 200
714 fmol of purified cDNA (Agencourt AMPure XP beads, *Beckman Coulter*™) from the
715 average fragment size identified were quantified using an Agilent Fragment Analyzer
716 and ligated. Only flow cells with at least 5,000 pores at the initial scan were used for
717 sequencing. Prepared library was loaded onto R10.4.1 flow cells (FLO-PRO114M,
718 *ONT*) on a PromethION P-48 device (*ONT*) (*Gustave Roussy Genomic Facility, Villejuif*
719 *France*) with MinKNOW (v6.0.14) and super high-accuracy base-calling mode.
720
721 **3' single-cell long read ONT sequencing analysis.**

722 Real-time base calling was run using MinKNOW (v7.4.14) with the Dorado basecaller
723 and the "Super-accurate basecalling v4.3.0" model. Alignments have been made using
724 the single-cell (v2.0.3) workflow from epi2me-labs (*https://github.com/epi2me-labs/wf-*
725 *single-cell*). After identification of the 10X adapters (from 3' V3.1 kit, *10X Genomics*)
726 and extraction of the cells barcodes and UMIs, the alignment on the human reference
727 (GRCh38-2024-A, *10X Genomics*) was performed using minimap2 (v2.24) as detailed
728 in the code, following parameters "-ax splice -uf --secondary=no". Genes and
729 transcripts assignment was performed using an in-house script from epi2me-labs
730 similar to FLAMES.
731 Cell barcode by symbol count table were loaded in R (version 4.1.0). To call real cells
732 from empty droplets, we used the emptyDrops() function from the dropletUtils package
733 (version 1.12.2), which assesses whether the RNA content associated with a cell
734 barcode is significantly distinct from the ambient background RNA present within each
735 sample. Barcodes with *p*-value < 0.001 (Benjamini-Hochberg-corrected) were
736 considered as legitimate cells for further analysis.
737 The count matrix was filtered to exclude genes detected in less than 5 cells, cells with
738 less than 1000 UMIs or less than 200 detected genes, as well as cells with
739 mitochondrial transcripts proportion >20%.The proportion of ribosomal gene counts
740 and the proportion of mechanical stress-response gene counts were also estimated
741 but not used to filter cells. Barcodes corresponding to doublet cells were identified and
742 discarded using the union of two methods: scDblFinder (version 1.6.0) and scds
743 (version 1.8.0) with its hybrid method with default parameters for both. We manually
744 verified that the cells identified as doublets did not systematically correspond to cells
745 in G2M phase.
746 Seurat (version 4.0.4) was applied for further data processing. The SCTransform
747 normalization method (Hafemeister & Satija Genome Biol. 2019) was used to
748 normalize, scale, select 3000 Highly Variable Genes and regress out bias factors
749 (nCount_RNA, the number of detected genes). Person residuals from this regression
750 were used for dimension reduction by Principal Component Analysis (PCA). The
751 number of PCA dimensions to keep for further analysis was evaluated by assessing a
752 range of reduced PCA spaces using 3 to 49 dimensions, with a step of 2. For each
753 generated PCA space, Louvain clustering of cells was performed using a range of
754 values for the resolution parameter from 0.1 to 1.2 with a step of 0.1. The optimal space
755 was manually evaluated as the one combination of kept dimensions and clustering

resolution resolving the best structure (clusters homogeneity and compacity) in a UMAP space. Additionally, we used the clustree method (version 0.4.3) to assess if the selected optimal space corresponded to a relatively stable position in the clustering results tested for these dimensions / resolution combinations.

An automatic annotation of cell types was performed by SingleR (version 1.6.1) (with fine-tuning step) and ClustifyR (version 1.5.1), using packages built-in references. It labels clusters (or cells) from a dataset based on similarity (Spearman correlation score) to a reference dataset with known labels. The labels with a correlation score greater than 0.25 for SingleR or greater than 0.35 for ClustifyR were kept. The annotation was made with CelliD (version 1.0.0) with genes signatures from panglao database. Marker genes for Louvain clusters were identified through a <U+00AB>one versus others<U+00BB> differential analysis using the Wilcoxon test through the FindAllMarkers() function (Seurat), considering only genes with a minimum log fold-change of 0.5 in at least 75% of cells from one of the groups compared, and FDR-adjusted p-values <0.05 (Benjaminin-Hochberg method). SNP were called by using bam-readcount on individual BAMs per barcodes.

Statistical analyses. Statistical analyses were performed with GraphPad Prism (version 10.3; *GraphPad Software Inc.*) or R packages using Mann-Whitney, Anova, Wilcoxon and Kruskal-Wallis tests, as indicated in figure legends. Unless otherwise stated, the data are expressed as mean±s.d. of n=3 or more determinations.

For xenotransplantation analysis, Kaplan–Meier survival curves were performed and the statistical significance was determined with the Log-rank (Mantel-Cox) test. Overall survival was defined as the time from cell injection to euthanasia or death at predefined endpoints. Animals were censored if the cause of death/sacrifice was not leukemia related. Number of mice and median survival are indicated into brackets.

For limiting dilution assays, statistical analysis was performed using the WEHI bioinformatic ELDA (Extreme Limiting Dilution Analysis) software[51]). Differences were considered statistically significant at p<0.05 (*), p<0.01 (**), p<0.001 (***) or p<0.0001 (****).

Authors' Contributions

Conception and design of the study: SG, EC and JS

Development of methodology: SG, SQ, LH, RJ, MA and JS

Acquisition of data (provided materials and animals, acquired and managed patients, provided facilities): SG, SQ, LH, LM, MP, RK, HB, MB, VP, PF, AB, HD, NB, EC and JS

Analysis and interpretation of data (biostatistics, computational analysis, statistical analysis): SG, SQ, LH, LM, MB, RJ, MA, FS, EC and JS

Writing of the manuscript - original draft preparation, review and editing: SG, HdT, EC and JS

Grants acquisition and study supervision: SG and JS

All authors critically reviewed the manuscript.

Disclosure of potential conflicts of interest

The authors declare no potential conflicts of interest.

Acknowledgments

The authors thank Niclas Setterblad, Christelle Doliger, Antonio Alberdi, Sophie Duchez and Claire Maillard from the Technological core facility of the Saint-Louis Research Institut, Inserm UMR1342 / CNRS EMR8000; Nathalie Droin and Maëla Francillette from the Genomic core facility of Gustave Roussy; the ICGex NGS platform of the Curie Institut for high-throughput sequencing of *10X* cDNA librairies.

Fundings

This work was supported by grants to Jean Soulier from the ERC St Grant Consolidator #311660, the team FRM 2022 program from the Fondation pour la Recherche Médicale #00107939, the Ligue Contre le Cancer IDF, the Fondation Leucémie Espoir, and by grants to Stéphanie Gachet from the Fondation de France, the Fondation ARC pour la Recherche sur le Cancer (PJA 20191209702), and the Paris Saint-Louis Leukemia Institute program (a grant managed by the French National Research Agency under the France 2030 program, ANR-23-IAHU-0005, Institut de la Leucémie Paris Saint-Louis). The ICGex platform was supported by the grants from the French National Research Agency, the Canceropole Ile-de-France and by the SiRIC-Curie program.

821

822 **Data-sharing statement**

823 The data that support the findings of this study are publically available at EBI
824 (https://www.ebi.ac.uk/biostudies) under the accession numbers BioStudies S-
825 BSST2554 and S-BSST2808, or in the Supplementary materials. The custom code
826 used for the analyses will be available on the published version of the article.

827

828 **REFERENCES**

829 1. Van Vlierberghe, P. & Ferrando, A. The molecular basis of T cell acute lymphoblastic leukemia. *J*
830 *Clin Invest* **122**, 3398–406 (2012).

831 2. Buckley, M., Yeung, D. T., White, D. L. & Eadie, L. N. T-cell acute lymphoblastic leukaemia: subtype
832 prevalence, clinical outcome, and emerging targeted treatments. *Leukemia* **39**, 1294–1310 (2025).

833 3. Weng, A. P. *et al.* Activating mutations of NOTCH1 in human T cell acute lymphoblastic leukemia.
834 *Science* **306**, 269–71 (2004).

835 4. Ferrando, A. A. *et al.* Gene expression signatures define novel oncogenic pathways in T cell acute
836 lymphoblastic leukemia. *Cancer Cell* **1**, 75–87 (2002).

837 5. Soulier, J. *et al.* HOXA genes are included in genetic and biologic networks defining human acute
838 T-cell leukemia (T-ALL). *Blood* **106**, 274–86 (2005).

839 6. Girardi, T., Vicente, C., Cools, J. & De Keersmaecker, K. The genetics and molecular biology of T-
840 ALL. *Blood* **129**, 1113–1123 (2017).

841 7. Pölönen, P. *et al.* The genomic basis of childhood T-lineage acute lymphoblastic leukaemia. *Nature*
842 **632**, 1082–1091 (2024).

843 8. Desjonqueres, A. *et al.* Acute lymphoblastic leukemia relapsing after first-line pediatric-inspired
844 therapy: a retrospective GRAALL study. *Blood Cancer J* **6**, e504 (2016).

845 9. Heikamp, E. B. & Pui, C. H. Next-Generation Evaluation and Treatment of Pediatric Acute
846 Lymphoblastic Leukemia. *J Pediatr* **203**, 14-24 e2 (2018).

847 10. Pagliaro, L. *et al.* Acute lymphoblastic leukaemia. *Nat. Rev. Dis. Primer* **10**, 41 (2024).

848 11. Brady, S. W. *et al.* The genomic landscape of pediatric acute lymphoblastic leukemia. *Nat. Genet.*
849 **54**, 1376–1389 (2022).

850 12. Pölönen, P., Mullighan, C. G. & Teachey, D. T. Classification and risk stratification in T-lineage
851 acute lymphoblastic leukemia. *Blood* **145**, 1464–1474 (2025).

852 13. Clappier, E. *et al.* Clonal selection in xenografted human T cell acute lymphoblastic leukemia
853 recapitulates gain of malignancy at relapse. *J Exp Med* **208**, 653–61 (2011).

854 14. Mullighan, C. G. *et al.* Genomic analysis of the clonal origins of relapsed acute lymphoblastic
855 leukemia. *Science* **322**, 1377–80 (2008).

856 15. Tosello, V. *et al.* WT1 mutations in T-ALL. *Blood* **114**, 1038–1045 (2009).

857 16. Anderson, K. *et al.* Genetic variegation of clonal architecture and propagating cells in leukaemia.
858 *Nature* **469**, 356–61 (2011).

859 17. Kunz, J. B. *et al.* Pediatric T-cell lymphoblastic leukemia evolves into relapse by clonal selection,
860 acquisition of mutations and promoter hypomethylation. *Haematologica* **100**, 1442–50 (2015).

861 18. Wong, T. N. *et al.* Role of TP53 mutations in the origin and evolution of therapy-related acute
862 myeloid leukaemia. *Nature* **518**, 552–555 (2015).

863 19. Oshima, K. *et al.* Mutational landscape, clonal evolution patterns, and role of RAS mutations in
864 relapsed acute lymphoblastic leukemia. *Proc Natl Acad Sci U A* **113**, 11306–11311 (2016).

865 20. Meyer, J. A. *et al.* Relapse-specific mutations in NT5C2 in childhood acute lymphoblastic leukemia.
866 *Nat. Genet.* **45**, 290–294 (2013).

867 21. Tzoneva, G. *et al.* Activating mutations in the NT5C2 nucleotidase gene drive chemotherapy
868 resistance in relapsed ALL. *Nat Med* **19**, 368–71 (2013).

869 22. Tzoneva, G. *et al.* Clonal evolution mechanisms in NT5C2 mutant-relapsed acute lymphoblastic
870 leukaemia. *Nature* **553**, 511–514 (2018).

871 23. Dieck, C. L. *et al.* Structure and Mechanisms of NT5C2 Mutations Driving Thiopurine Resistance in
872 Relapsed Lymphoblastic Leukemia. *Cancer Cell* **34**, 136-147.e6 (2018).

873 24. Barz, M. J. *et al.* Subclonal NT5C2 mutations are associated with poor outcomes after relapse of
874 pediatric acute lymphoblastic leukemia. *Blood* **135**, 921–933 (2020).

875 25. Diccianni, M. B. *et al.* Clinical significance of p53 mutations in relapsed T-cell acute lymphoblastic
876 leukemia. *Blood* **84**, 3105–12 (1994).

877 26. Hof, J. *et al.* Mutations and deletions of the TP53 gene predict nonresponse to treatment and poor
878 outcome in first relapse of childhood acute lymphoblastic leukemia. *J Clin Oncol* **29**, 3185–93
879 (2011).

880 27. Hof, J. *et al.* NOTCH1 mutation, TP53 alteration and myeloid antigen expression predict outcome
881 heterogeneity in children with first relapse of T-cell acute lymphoblastic leukemia. *Haematologica*
882 **102**, e249–e252 (2017).

883 28. Richter-Pechańska, P. *et al.* Identification of a genetically defined ultra-high-risk group in relapsed
884 pediatric T-lymphoblastic leukemia. *Blood Cancer J.* **7**, e523 (2017).

885 29. Simonin, M. *et al.* Prognostic value and oncogenic landscape of TP53 alterations in adult and
886 pediatric T-ALL. *Blood* **141**, 1353–1358 (2023).

887 30. Kempter, T. *et al.* Subclonal TP53 and KRAS variants combined with poor treatment response
888 identify ultrahigh-risk pediatric patients with T-ALL. *Blood Adv.* **9**, 1267–1279 (2025).

889 31. Li, B. *et al.* Therapy-induced mutations drive the genomic landscape of relapsed acute
890 lymphoblastic leukemia. *Blood* https://doi.org/10.1182/blood.2019002220 (2020)
891 doi:10.1182/blood.2019002220.

892 32. Armstrong, F. *et al.* NOTCH is a key regulator of human T-cell acute leukemia initiating cell activity.
893 *Blood* **113**, 1730–1740 (2009).

894 33. Liu, Y., Su, Z., Tavana, O. & Gu, W. Understanding the complexity of p53 in a new era of tumor
895 suppression. *Cancer Cell* **42**, 946–967 (2024).

896 34. Dong, Y., Tu, R., Liu, H. & Qing, G. Regulation of cancer cell metabolism: oncogenic MYC in the
897 driver's seat. *Signal Transduct. Target. Ther.* **5**, 124 (2020).

898 35. Richter-Pechańska, P. *et al.* Pediatric T-ALL type-1 and type-2 relapses develop along distinct
899 pathways of clonal evolution. *Leukemia* **36**, 1759–1768 (2022).

900 36. Albertí-Servera, L. *et al.* Single-cell DNA amplicon sequencing reveals clonal heterogeneity and
901 evolution in T-cell acute lymphoblastic leukemia. *Blood* **137**, 801–811 (2021).

902 37. Calvo, J. *et al.* High CD44 expression and enhanced E-selectin binding identified as biomarkers of
903 chemoresistant leukemic cells in human T-ALL. *Leukemia* **39**, 323–336 (2025).

904 38. Xu, J. *et al.* A multiomic atlas identifies a treatment-resistant, bone marrow progenitor-like cell
905 population in T cell acute lymphoblastic leukemia. *Nat. Cancer* **6**, 102–122 (2025).

906 39. Ebinger, S. *et al.* Characterization of Rare, Dormant, and Therapy-Resistant Cells in Acute
907 Lymphoblastic Leukemia. *Cancer Cell* **30**, 849–862 (2016).

908 40. Costea, J. *et al.* Role of stem-like cells in chemotherapy resistance and relapse in pediatric T-cell
909 acute lymphoblastic leukemia. *Nat. Commun.* **16**, 5413 (2025).

910 41. Hsu, J. I. *et al.* PPM1D Mutations Drive Clonal Hematopoiesis in Response to Cytotoxic
911 Chemotherapy. *Cell Stem Cell* **23**, 700-713.e6 (2018).

912 42. Chen, S. *et al.* Mutant p53 drives clonal hematopoiesis through modulating epigenetic pathway.
913 *Nat. Commun.* **10**, 5649 (2019).

914 43. Liu, Y., Su, Z., Tavana, O. & Gu, W. Understanding the complexity of p53 in a new era of tumor
915 suppression. *Cancer Cell* **42**, 946–967 (2024).

916 44. Chomczyk, M. *et al.* Impact of p53-associated acute myeloid leukemia hallmarks on metabolism
917 and the immune environment. *Front. Pharmacol.* **15**, 1409210 (2024).

918 45. Chiu, P. P. L., Jiang, H. & Dick, J. E. Leukemia-initiating cells in human T-lymphoblastic leukemia
919 exhibit glucocorticoid resistance. *Blood* **116**, 5268–5279 (2010).

920 46. Belmonte, M., Hoofd, C., Weng, A. P. & Giambra, V. Targeting leukemia stem cells: which pathways
921 drive self-renewal activity in T-cell acute lymphoblastic leukemia? *Curr Oncol* **23**, 34–41 (2016).

922 47. Gerby, B. *et al.* High-throughput screening in niche-based assay identifies compounds to target
923 preleukemic stem cells. *J. Clin. Invest.* **126**, 4569–4584 (2016).

48. Yadav, B. D. *et al.* Heterogeneity in mechanisms of emergent resistance in pediatric T-cell acute lymphoblastic leukemia. *Oncotarget* **7**, 58728–42 (2016).

49. Ariës, I. M. *et al.* PRC2 loss induces chemoresistance by repressing apoptosis in T cell acute lymphoblastic leukemia. *J. Exp. Med.* **215**, 3094–3114 (2018).

50. Gachet, S. *et al.* Deletion 6q Drives T-cell Leukemia Progression by Ribosome Modulation. *Cancer Discov* **8**, 1614–1631 (2018).

51. Hu, Y. & Smyth, G. K. ELDA: extreme limiting dilution analysis for comparing depleted and enriched populations in stem cell and other assays. *J. Immunol. Methods* **347**, 70–78 (2009).

52. Ceccaldi, R. *et al.* Bone marrow failure in Fanconi anemia is triggered by an exacerbated p53/p21 DNA damage response that impairs hematopoietic stem and progenitor cells. *Cell Stem Cell* **11**, 36–49 (2012).

53. Sebert, M. *et al.* Clonal hematopoiesis driven by chromosome 1q/MDM4 trisomy defines a canonical route toward leukemia in Fanconi anemia. *Cell Stem Cell* **30**, 153-170.e9 (2023).

54. Gerby, B. *et al.* Optimized gene transfer into human primary leukemic T cell with NOD-SCID/leukemia-initiating cell activity. *Leukemia* **24**, 646–9 (2010).

55. Mihara, K. *et al.* Development and functional characterization of human bone marrow mesenchymal cells immortalized by enforced expression of telomerase. *Br. J. Haematol.* **120**, 846–849 (2003).

56. Patel, A. P. *et al.* Single-cell RNA-seq highlights intratumoral heterogeneity in primary glioblastoma. *Science* **344**, 1396–1401 (2014).

57. Zhu, Q. *et al.* Single cell multi-omics reveal intra-cell-line heterogeneity across human cancer cell lines. *Nat. Commun.* **14**, 8170 (2023).

947 **FIGURE LEGENDS**

948 **Figure 1. *In vivo* isogenic modelling of diagnosis and relapse *TP53*-altered T-**
949 **ALL. A.** Experimental design (Created in BioRender. Gachet, S. (2026)
950 https://BioRender.com/zczr8er). Isogenic Dx-Rel PDX pairs were established after
951 injection into immunodeficient NSG mice of paired primary diagnosis and *TP53*-altered
952 (*TP53*^{alt}) relapse samples from the same T-ALL patients. **B.** Comparative Whole
953 Exome Sequencing (WES) analysis of the isogenic Dx-Rel PDX samples established
954 from 4 T-ALL patients who relapsed with *17p/TP53* alterations. In each case, PDX
955 samples (PDXD and PDXR) are compared side-by-side to the corresponding primary
956 samples (TALLD and TALLR, respectively). **C.** Lollipop plot of *TP53* mutations
957 observed in 4 primary relapse samples (TALL11R, TALL30R, TALL42R and
958 TALL43R).

959

960 **Figure 2. *TP53*^{alt} T-ALL relapse cells display a cell-intrinsic gain of malignancy**
961 **phenotype. A.** Kaplan-Meier survival curves of PDX mice engrafted with primary
962 isogenic Dx-Rel leukemic cells from 4 T-ALL patients (TALL11, TALL30, TALL42 and
963 TALL43). N=4-5 recipient mice injected at equivalent cell doses per sample. **B-C.**
964 Parallel serial transplantations of paired Dx-Rel T-ALL PDX samples. Kaplan-Meier
965 survival curves of mice injected with 3 cell doses (10^6, 10^5 and 10^4 cells) of isogenic
966 Dx-Rel PDX pairs (n = 4 TALL cases) raised from primary (**B**) and secondary (**C**)
967 xenografts. **D.** LIC frequencies of isogenic Dx-Rel PDX sample pairs calculated from
968 *in vivo* limiting dilutions. **E-F.** Real-time *in vitro* cell proliferation and apoptosis of
969 leukemic cells from isogenic Dx-Rel PDX pairs, measured with the Incucyte® Live-Cell
970 Analysis System. Proliferation was quantified by measuring the proportion of phase
971 objects confluence over time, without labels **(E)**, and apoptosis by the quantification of
972 green fluorescently labelled nuclei after activated caspase-3/7 cleavage of inert
973 Incucyte® Caspase-3/7 dyes **(F)**.
974 Statistical data in this figure are represented as mean ± s.d. Significance is indicated
975 by *P* values; A-C: Log-rank test (Mantel-Cox); D: overall tests for differences using
976 ELDA software; E-F: two-way Anova test. Number of recipient mice and median
977 survival are indicated into brackets on Kaplan-Meier survival curves. ns, not significant;
978 *, $p < 0.05$; **, $p < 0.01$; ***, $p < 0.001$; ****, $p < 0.0001$.

979

980 **Figure 3. *TP53* silencing confers a relapse phenotype to diagnosis leukemic**
981 **cells. A.** Experimental design of *TP53* silencing in diagnosis cells from PDX samples
982 using a lentiviral shRNA approach (Created in BioRender. Gachet, S. (2026)
983 https://BioRender.com/usb6t9c). **B-C.** Primary transplantation of paired control
984 mCherry$^+$ (shCTL mCherry) and *TP53* KD GFP$^+$ (sh *TP53* GFP) leukemic cells from
985 PDX30D injected in parallel settings into recipient mice. **B.** Engraftment kinetics in the
986 bone marrow (BM) of recipient mice (n=6) injected with paired control and *TP53* KD
987 leukemic cells from PDX30D. **C.** Kaplan-Meier survival curves of mice injected with
988 paired control and *TP53* KD leukemic cells from PDX30D. **D-F.** Secondary transplant
989 of paired control mCherry$^+$ (shCTL mCherry) and *TP53* KD GFP$^+$ (sh *TP53* GFP)
990 leukemic cells from PDX30D injected either in parallel (panels D-E) or competitive
991 (panel F) settings into recipient mice. **D.** Engraftment kinetics in the BM of recipient
992 mice (n=5) injected in parallel settings with cells from control and *TP53* KD conditions.
993 **E.** Kaplan-Meier survival curves of mice injected in parallel settings with sorted control
994 or *TP53* KD leukemic cells from PDX30D. **F.** Engraftment kinetics in the BM of recipient
995 mice (n=4) injected with sorted cells from both control and *TP53* KD in competitive
996 settings (ratio 1:1). Data are represented as ratios of *TP53* KD GFP$^+$ over control
997 mCherry$^+$ leukemic cells within BM of the same recipient mouse and compared to the
998 input. **G.** LIC frequencies of paired control-*TP53* KD samples calculated from *in vitro*
999 long-term culture-initiating cell assays of sorted GFP$^+$ or mCherry$^+$ CD45$^+$CD7$^+$
1000 leukemic cell from diagnosis PDX samples (PDX30D and PDX42D). LIC frequencies
1001 are estimated based on the proportions of positive wells for GFP$^+$/mCherry$^+$
1002 CD45$^+$CD7$^+$ leukemic cells evaluated after 2 and 4 weeks of culture.
1003 Statistical data in this figure are represented as mean ± s.d. Significance is indicated
1004 by *P* values; B and D: Mann-Whitney test; C and E: Log-rank test (Mantel-Cox); F:
1005 Kruskal-Wallis test; G: overall tests for differences using ELDA software. Number of
1006 recipient mice and median survival are indicated into brackets on Kaplan-Meier
1007 survival curves. ns, not significant; *, $p < 0.05$; **, $p < 0.01$; ****, $p < 0.0001$.
1008
1009 **Figure 4. *TP53* alterations drive a relapse phenotype through MYC signaling and**
1010 **metabolism deregulation. A.** Supervised hierarchical clustering of the top fifty most
1011 differentially expressed genes between Dx and Rel T-ALL samples. Heatmap
1012 representation of the most variables genes at Dx and Rel in 4 isogenic PDX pairs
1013 (primografts). *TP53* expression is highlighted in red. Independent triplicates are

1014 analysed for each isogenic PDX pair. **B-C.** GSEA of enriched pathways in *TP53*^{alt} T-
1015 ALL relapse samples. **B.** Comparative Gene Set Enrichment Analysis (GSEA) of
1016 differentially expressed genes in Rel and Dx samples from 4 isogenic PDX pairs.
1017 Representation of selected Hallmark pathways significantly upregulated at relapse,
1018 defining a relapse expression signature in all isogenic Dx-Rel PDX pairs pooled
1019 together (1st column "All_PDXs") and in each individual PDX pair (2nd to 5th columns;
1020 respectively PDX11, PDX30, PDX42 and PDX43) (*P* adj <0.05). **C.** GSEA of the
1021 upregulated (upper panel) and downregulated (lower panel) relapse expression
1022 signature obtained from PDX samples (panel B) tested in the original T-ALL patients
1023 samples. UP_PDX, upregulated transcriptomic signature in Rel PDXs; DOWN_PDX,
1024 downregulated transcriptomic signature in Rel PDXs. FDR, false discovery rate; NES,
1025 normalized enrichment score. **D-G.** Direct evaluation of mitochondrial respiration in
1026 leukemic cells from isogenic Dx-Rel PDXs using Seahorse assays. **D.** Real-time
1027 measurements of oxygen consumption rate (OCR) in isogenic Dx-Rel leukemic cells
1028 from 4 T-ALL cases. **E.** Quantification of maximal respiration in leukemic cells from 4
1029 isogenic Dx-Rel PDX pairs evaluated in 3 independent experiments. **F.** Real-time
1030 measurements of OCR in *TP53*-silenced (*TP53* KD) and matched control leukemic
1031 cells from diagnosis PDX samples (PDX42D and PDX43D). **G.** Quantification of
1032 maximal respiration in *TP53* KD and control leukemic cells from 3 independent
1033 diagnosis PDX samples (PDX30D, PDX42D and PDX43D) evaluated in 2 independent
1034 experiments
1035 Statistical data in this figure are represented as mean ± s.d. Significance is indicated
1036 by *P* values; E and G: Mann-Whitney test. ns, not significant; **, $p < 0.01$; ***, $p <$
1037 0.001; ****, $p < 0.0001$.
1038
1039 **Figure 5. Single-cell profiling of isogenix Dx-Rel T-ALLs can unveil a pre-relapse**
1040 **cells reservoir at diagnosis. A.** UMAP visualizations of isogenic Dx-Rel primary
1041 samples from 4 T-ALL patients and their derived PDXs analysed by short read single-
1042 cell RNA (scRNA) sequencing. UMAP plots of 117.119 single cells coloured by T-ALL
1043 samples (n=16, primary and PDXs samples from 4 T-ALL cases at diagnosis and
1044 relapse; left panel), leukemic cell identity (Diagnosis versus Relapse; middle panel)
1045 and by leukemic cell origin (Primary versus PDX; right panel). **B-C.** GSEA of biological
1046 pathways enriched at relapse in primary and PDX T-ALL samples. GSEA from pseudo
1047 bulk analysis of differentially expressed genes between relapse (Rel) and diagnosis

1048 (Dx) samples from isogenic patient (**B**) and PDX (**C**) T-ALL pairs retrieves the relapse
1049 expression signature defined in Figure 4B. Representation of selected Hallmark
1050 pathways significantly deregulated at relapse (*P* adj <0.05) in all isogenic pairs pooled
1051 together (1st column ") and in each individual pair (2nd to 5th columns). Note that TALL30
1052 case eventually diverged from the other cases by the late acquisition of a *NT5C2*
1053 mutation, known to drive resistance to maintenance therapy. **D.** Oncogenetic
1054 trajectories for diagnosis and relapse TALL42 and TALL30 samples. **E.** UMAP
1055 visualizations of Dx and Rel primary samples from TALL42 case analysed by short
1056 read scRNA sequencing. UMAP plots of 14.049 single leukemic cells coloured by cell
1057 identity (Diagnosis vs Relapse; upper panel) and cluster-based by transcriptomic data
1058 (fourteen different clusters; lower panel). The red dotted ellipse highlights cluster 6 in
1059 TALL42D sample. **F.** Dot plot visualization of biomarker genes average expression
1060 selected from the unsupervised differential expression analysis between Rel and Dx
1061 samples from TALL42 case. Average expression and proportion of expressing cells for
1062 selected biomarkers are represented in each cluster from Dx and Rel samples. The
1063 red dotted line highlights the pre-relapse cells reservoir. **G-H.** GSEA of positively and
1064 negatively enriched pathways at relapse and pre-relapse stages in TALL42 samples.
1065 **G.** Representation of selected Hallmark pathways significantly deregulated in relapse
1066 (1st column Rel vs Dx; *P* adj <0.05) and pre-relapse (2nd column Sub vs Dx, red dotted
1067 line; *P* adj <0.05) clusters as compared to matched diagnosis counterparts. **H.**
1068 Representation of specific gene sets from the MSigDB C1 and C2 collections
1069 significantly upregulated (in red) or downregulated (in blue) at relapse (1st column Rel
1070 vs Dx; *P* adj <0.05) and pre-relapse (2nd column Sub vs Dx; *P* adj <0.05) as compared
1071 to matched primary diagnosis counterparts. Color code indicates the cell proliferation,
1072 invasiveness, stemness and oxidative phosphorylation signatures. **I** Single-cell scores
1073 for several leukemia stem cell (LSC) signatures in TALL42 diagnosis (Dx), pre-relapse
1074 (Sub) and relapse (Rel) clusters. The box includes the median, hinges mark the 25th
1075 and 75th percentiles. *P* values from a two-sided paired t-test are shown. ns, not
1076 significant; ****, $p < 0.0001$ **J.** UMAP visualizations of Dx and Rel primary samples
1077 from TALL42 case analysed by long read single-cell RNA sequencing. UMAP plots of
1078 14.883 single leukemic cells (8.861 cells from diagnosis and 6.022 cells from relapse)
1079 coloured by cell identity (Diagnosis vs Relapse; left panel) and cluster-based by
1080 transcriptomic data (9 different clusters corresponding to leukemic cells; right panel).
1081 **K.** Projection of *TP53* WT and mutant (*TP53*-R175H*)* reads at chromosomal location

1082 chr17:7’675’088 (hg38) from TALL42 Dx and Rel samples. **L.** Quantification of *TP53*
1083 mutant reads retrived in isogenic Dx (6/193) and Rel (35/35) TALL42 samples. **M.**
1084 Single-cell signature scores for relevant hallmark pathways of the relapse expression
1085 signature (OXPHOS, MYC target V1 and MTORC1 signaling) in *TP53* WT and mutant
1086 cells. The box includes the median, hinges mark the 25th and 75th percentiles.
1087

Figure 1

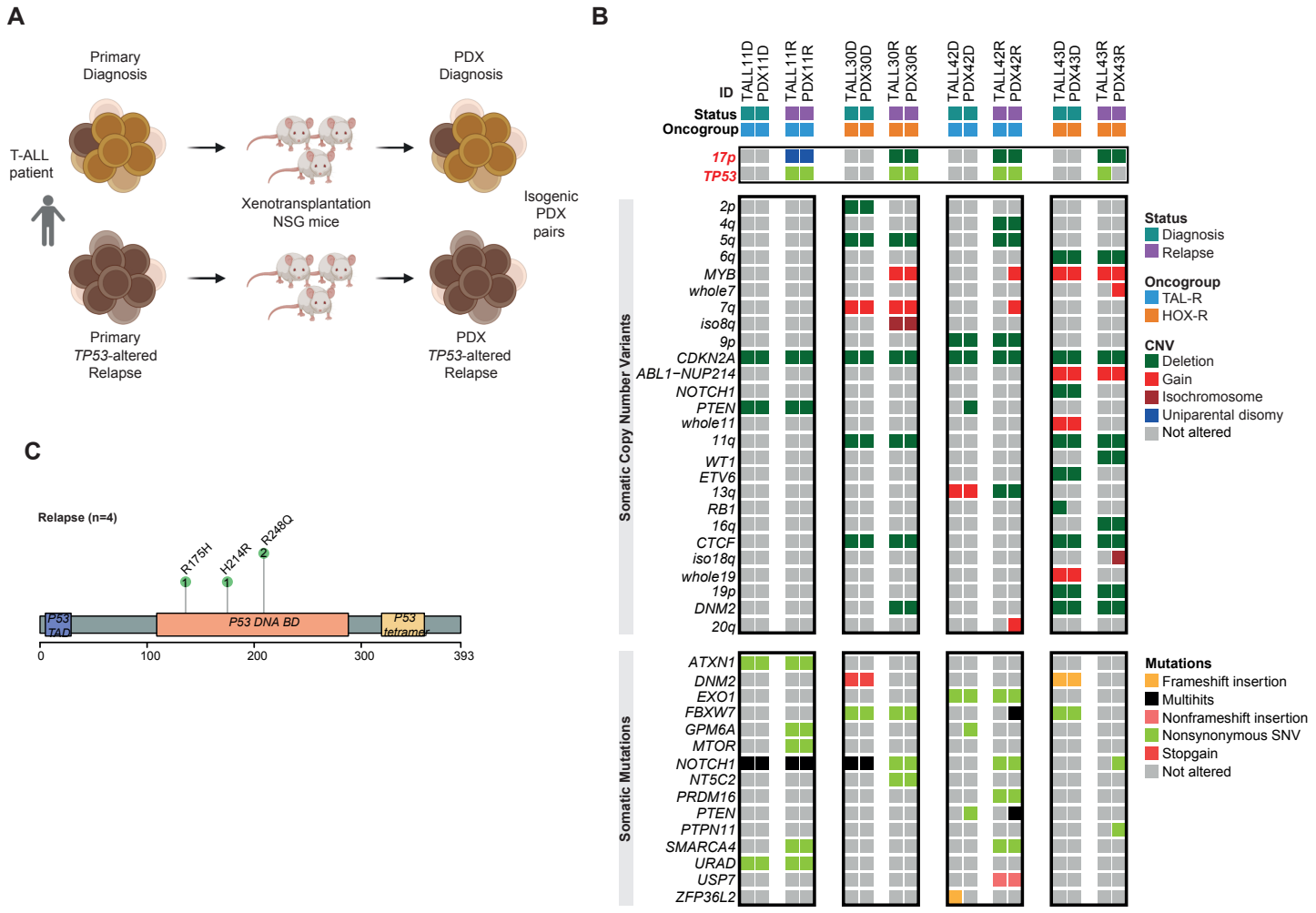
A
Primary Diagnosis
PDX Diagnosis
T-ALL patient
Xenotransplantation NSG mice
Isogenic PDX pairs
Primary TP53-altered Relapse
PDX TP53-altered Relapse
B
ID
TALL11D PDX11D
TALL11R PDX11R
TALL30D PDX30D
TALL30R PDX30R
TALL42D PDX42D
TALL42R PDX42R
TALL43D PDX43D
TALL43R PDX43R
Status
Oncogroup
17p
TP53
Somatic Copy Number Variants
2p
4q
5q
6q
MYB
whole7
7q
iso8q
9p
CDKN2A
ABL1−NUP214
NOTCH1
PTEN
whole11
11q
WT1
ETV6
13q
RB1
16q
CTCF
iso18q
whole19
19p
DNM2
20q
Status
Diagnosis
Relapse
Oncogroup
TAL-R
HOX-R
CNV
Deletion
Gain
Isochromosome
Uniparental disomy
Not altered
Somatic Mutations
ATXN1
DNM2
EXO1
FBXW7
GPM6A
MTOR
NOTCH1
NT5C2
PRDM16
PTEN
PTPN11
SMARCA4
URAD
USP7
ZFP36L2
Mutations
Frameshift insertion
Multihits
Nonframeshift insertion
Nonsynonymous SNV
Stopgain
Not altered
C
Relapse (n=4)
R175H
H214R
R248Q
P53 TAD
P53 DNA BD
P53 tetramer
0
100
200
300
393

Figure 2

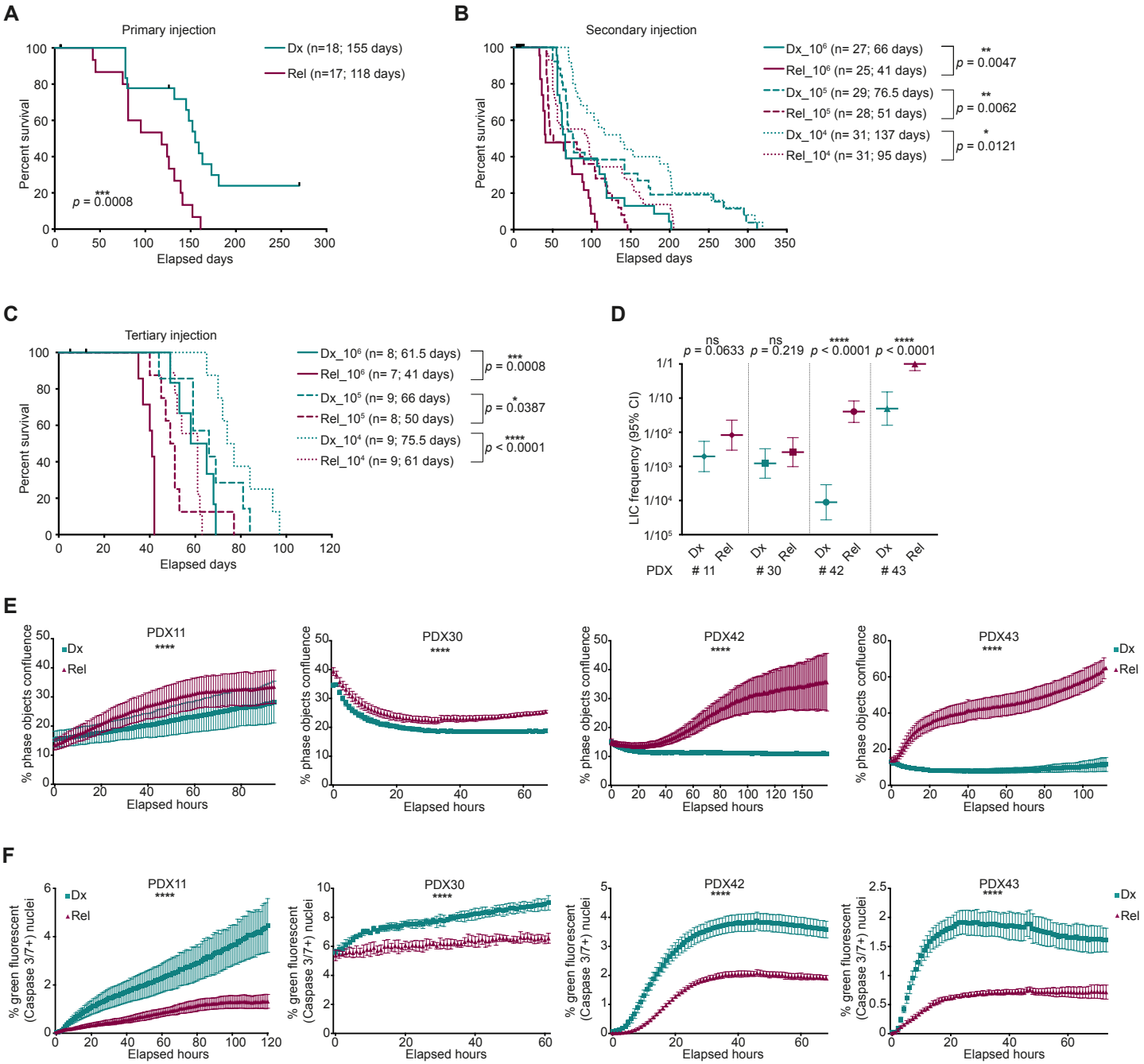
A
Primary injection
Dx (n=18; 155 days)
Rel (n=17; 118 days)
p = 0.0008
Percent survival
Elapsed days
B
Secondary injection
Dx_10⁶ (n= 27; 66 days)
Rel_10⁶ (n= 25; 41 days)
p = 0.0047
Dx_10⁵ (n= 29; 76.5 days)
Rel_10⁵ (n= 28; 51 days)
p = 0.0062
Dx_10⁴ (n= 31; 137 days)
Rel_10⁴ (n= 31; 95 days)
p = 0.0121
C
Tertiary injection
Dx_10⁶ (n= 8; 61.5 days)
Rel_10⁶ (n= 7; 41 days)
p = 0.0008
Dx_10⁵ (n= 9; 66 days)
Rel_10⁵ (n= 8; 50 days)
p = 0.0387
Dx_10⁴ (n= 9; 75.5 days)
Rel_10⁴ (n= 9; 61 days)
p < 0.0001
D
p = 0.0633 p = 0.219 p < 0.0001 p < 0.0001
LIC frequency (95% CI)
PDX # 11 # 30 # 42 # 43
E
PDX11
PDX30
PDX42
PDX43
% phase objects confluence
Elapsed hours
F
% green fluorescent (Caspase 3/7+) nuclei
Elapsed hours

Figure 3

A

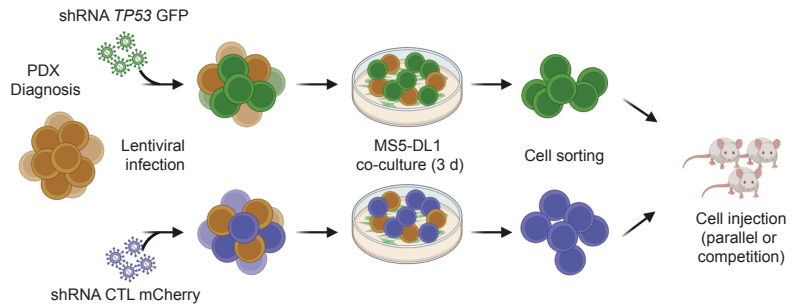

B

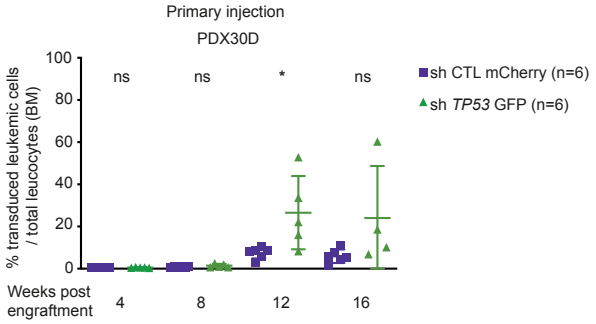

C

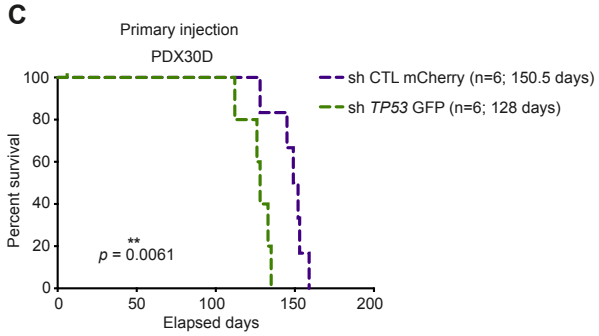

D

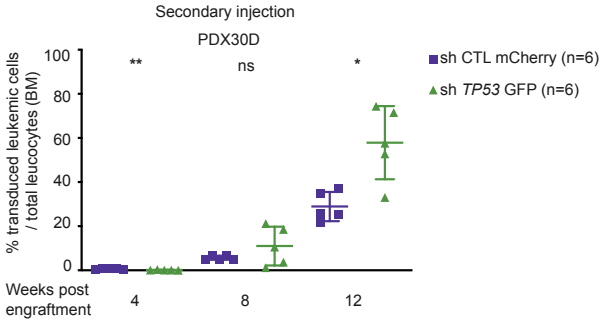

E

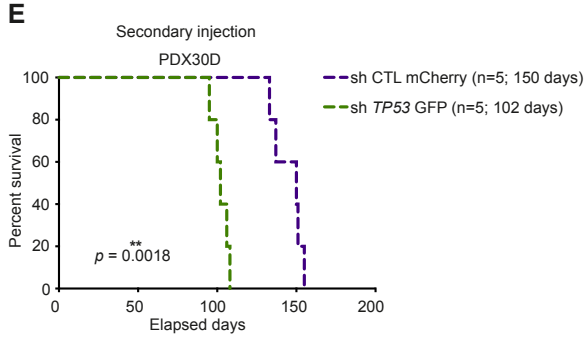

F

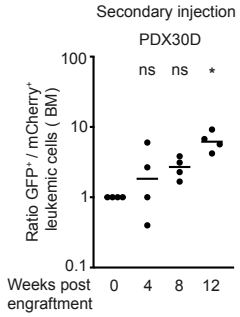

G

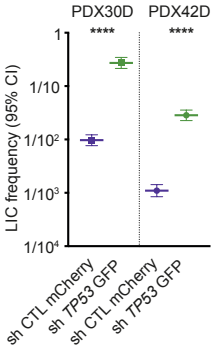

Figure 4

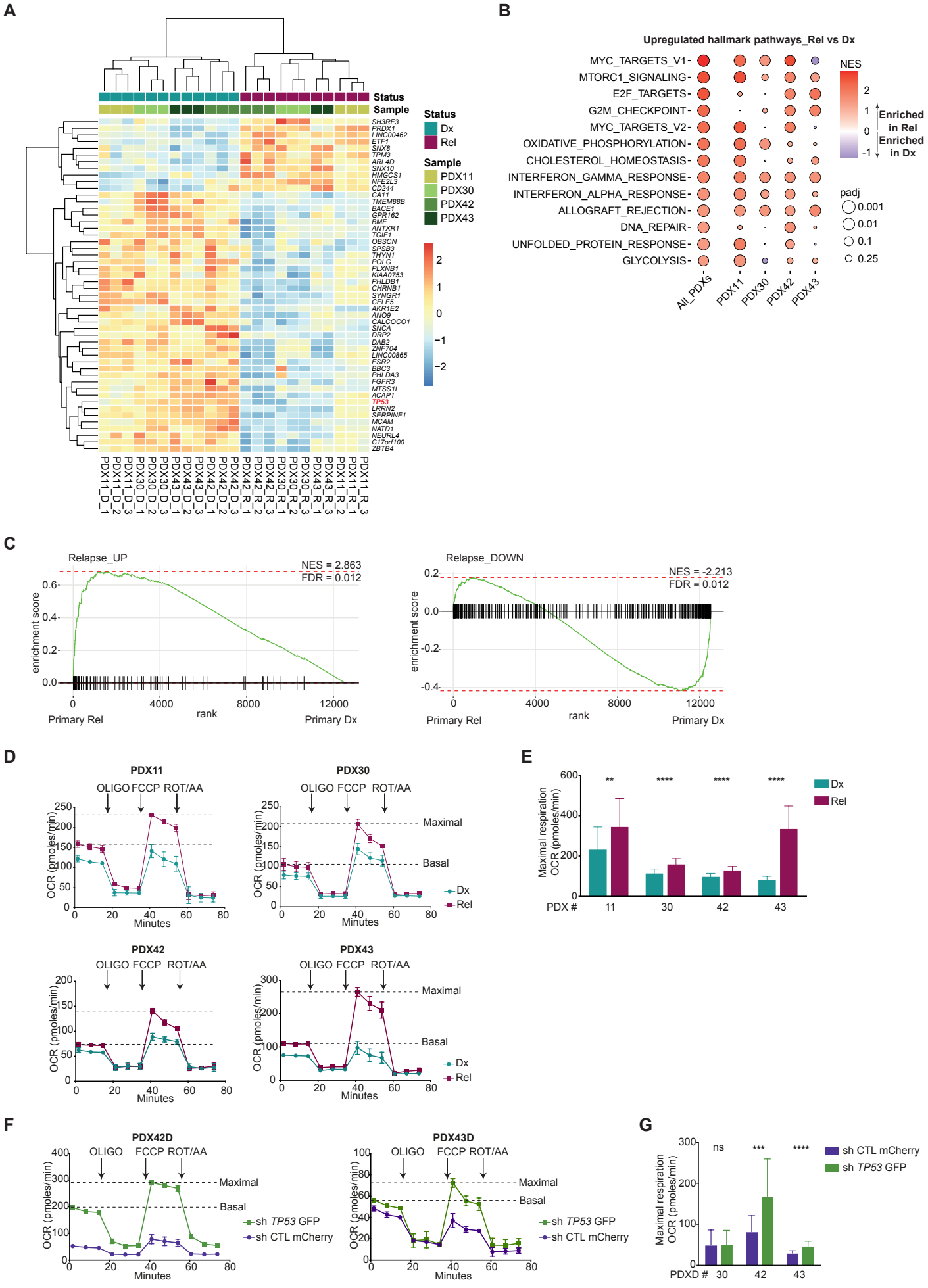
A
Status
Sample
Status
Dx
Rel
Sample
PDX11
PDX30
PDX42
PDX43
SH3RF3
PRDX1
LINC00462
ETF1
SNX8
TPM3
ARL4D
SNX10
HMGCS1
NFE2L3
CD244
CA11
TMEM88B
BACE1
GPR162
BMF
ANTXR1
TGIF1
OBSCN
SPSB3
THYN1
POLG
PLXNB1
KIAA0753
PHLDB1
CHRNB1
SYNGR1
CELF5
AKR1E2
ANO9
CALCOCO1
SNCA
DRP2
DAB2
ZNF704
LINC00865
ESR2
BBC3
PHLDA3
FGFR3
MTSS1L
ACAP1
TP53
LRRN2
SERPINF1
MCAM
NATD1
NEURL4
C17orf100
ZBTB4
PDX11_D_1
PDX11_D_2
PDX11_D_3
PDX30_D_1
PDX30_D_2
PDX30_D_3
PDX43_D_1
PDX43_D_2
PDX43_D_3
PDX42_D_1
PDX42_D_2
PDX42_D_3
PDX42_R_1
PDX42_R_2
PDX42_R_3
PDX30_R_1
PDX30_R_2
PDX30_R_3
PDX43_R_1
PDX43_R_2
PDX43_R_3
PDX11_R_1
PDX11_R_2
PDX11_R_3
B
Upregulated hallmark pathways_Rel vs Dx
MYC_TARGETS_V1
MTORC1_SIGNALING
E2F_TARGETS
G2M_CHECKPOINT
MYC_TARGETS_V2
OXIDATIVE_PHOSPHORYLATION
CHOLESTEROL_HOMEOSTASIS
INTERFERON_GAMMA_RESPONSE
INTERFERON_ALPHA_RESPONSE
ALLOGRAFT_REJECTION
DNA_REPAIR
UNFOLDED_PROTEIN_RESPONSE
GLYCOLYSIS
All_PDXs
PDX11
PDX30
PDX42
PDX43
NES
Enriched in Rel
Enriched in Dx
padj
0.001
0.01
0.1
0.25
C
Relapse_UP
NES = 2.863
FDR = 0.012
enrichment score
rank
Primary Rel
Primary Dx
Relapse_DOWN
NES = -2.213
FDR = 0.012
D
PDX11
PDX30
PDX42
PDX43
OLIGO FCCP ROT/AA
OCR (pmoles/min)
Minutes
Maximal
Basal
Dx
Rel
E
Maximal respiration OCR (pmoles/min)
PDX #
F
PDX42D
PDX43D
OLIGO FCCP ROT/AA
sh TP53 GFP
sh CTL mCherry
G
Maximal respiration OCR (pmoles/min)
PDXD #
ns
sh CTL mCherry
sh TP53 GFP

Figure 5

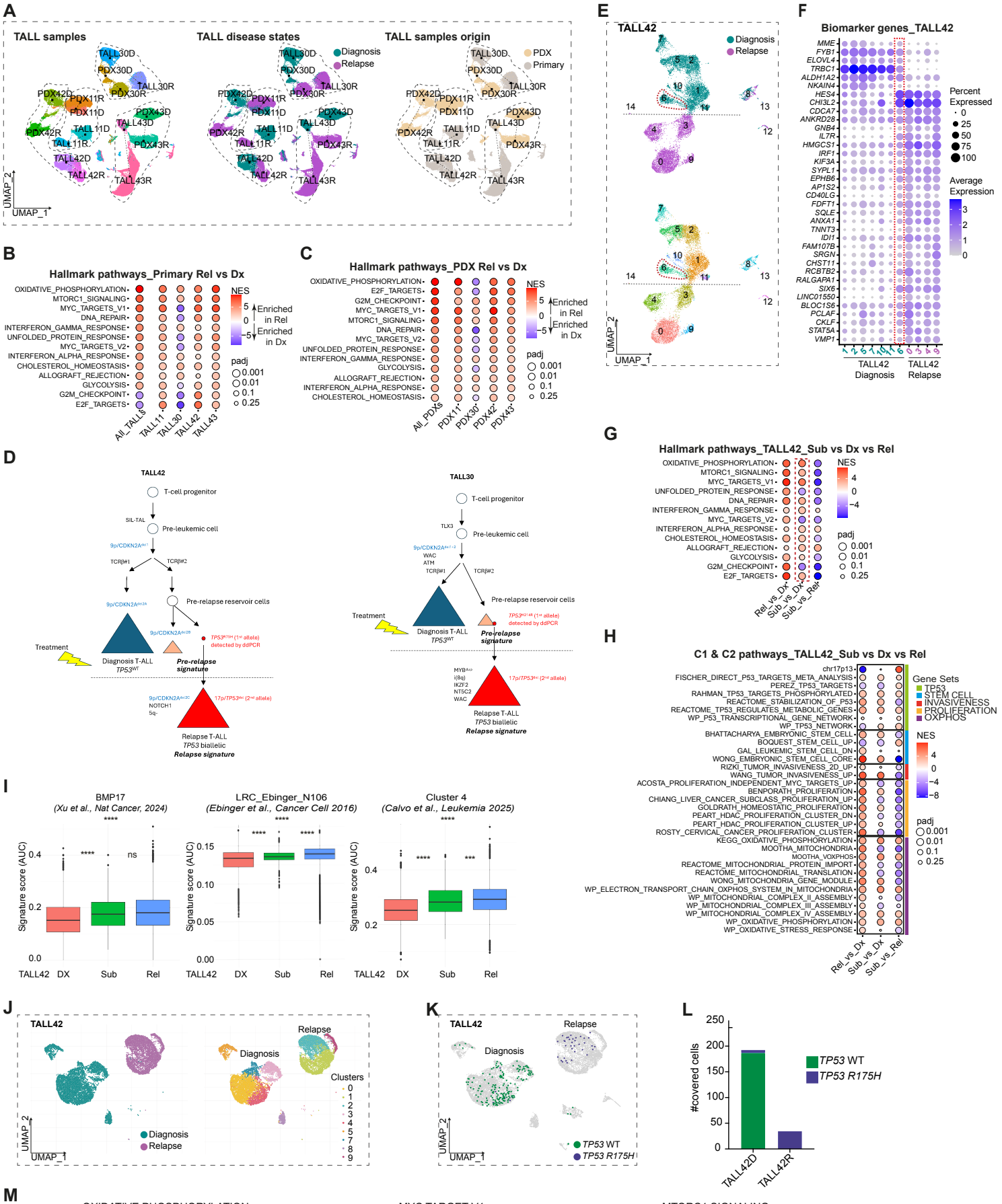
A
TALL samples
TALL disease states
TALL samples origin
Diagnosis
Relapse
PDX
Primary
UMAP_1
UMAP_2
B
Hallmark pathways_Primary Rel vs Dx
OXIDATIVE_PHOSPHORYLATION
MTORC1_SIGNALING
MYC_TARGETS_V1
DNA_REPAIR
INTERFERON_GAMMA_RESPONSE
UNFOLDED_PROTEIN_RESPONSE
MYC_TARGETS_V2
INTERFERON_ALPHA_RESPONSE
CHOLESTEROL_HOMEOSTASIS
ALLOGRAFT_REJECTION
GLYCOLYSIS
G2M_CHECKPOINT
E2F_TARGETS
All_TALLS
TALL11
TALL30
TALL42
TALL43
NES
Enriched in Rel
Enriched in Dx
padj
C
Hallmark pathways_PDX Rel vs Dx
OXIDATIVE_PHOSPHORYLATION
E2F_TARGETS
G2M_CHECKPOINT
MYC_TARGETS_V1
MTORC1_SIGNALING
DNA_REPAIR
MYC_TARGETS_V2
UNFOLDED_PROTEIN_RESPONSE
INTERFERON_GAMMA_RESPONSE
GLYCOLYSIS
ALLOGRAFT_REJECTION
INTERFERON_ALPHA_RESPONSE
CHOLESTEROL_HOMEOSTASIS
All_PDXs
PDX11
PDX30
PDX42
PDX43
D
TALL42
T-cell progenitor
Pre-leukemic cell
Pre-relapse reservoir cells
Treatment
Diagnosis T-ALL
Pre-relapse signature
Relapse T-ALL
TP53 biallelic
Relapse signature
TALL30
E
TALL42
Diagnosis
Relapse
F
Biomarker genes_TALL42
Percent Expressed
Average Expression
TALL42 Diagnosis
TALL42 Relapse
G
Hallmark pathways_TALL42_Sub vs Dx vs Rel
Rel_vs_Dx
Sub_vs_Dx
Sub_vs_Rel
H
C1 & C2 pathways_TALL42_Sub vs Dx vs Rel
Gene Sets
TP53
STEM CELL
INVASIVENESS
PROLIFERATION
OXPHOS
I
BMP17
(Xu et al., Nat Cancer, 2024)
LRC_Ebinger_N106
(Ebinger et al., Cancer Cell 2016)
Cluster 4
(Calvo et al., Leukemia 2025)
Signature score (AUC)
TALL42
DX
Sub
Rel
J
TALL42
Clusters
K
TALL42
Diagnosis
Relapse
TP53 WT
TP53 R175H
L
#covered cells
TALL42D
TALL42R
M
OXIDATIVE PHOSPHORYLATION
MYC TARGET V1
MTORC1 SIGNALING
Signature score (AUC)
no cell
TALL42
Dx_TP53 WT
Dx_TP53 mut
Rel_TP53 WT
Rel_TP53 mut